Modeling of the immune response during virus infection of the human respiratory tract

Mikaela Giegold

2018

LUND
UNIVERSITY

CBG
Max Planck Institute
of Molecular Cell Biology
and Genetics

center for
systems biology
dresden

Masters Thesis in
Biomedical Engineering

Faculty of Engineering LTH
Department of Biomedical Engineering

Supervisors:
Tobias Ambjörnsson
Anders Brodin
Ivo Sbalzarini

Abstract

Respiratory virus infections are associated with Chronic Obstructive Pulmonary Disease (COPD) exacerabtions. Human Rhinovirus (HRV) has been found in many exacerbations and is believed to be a triggering factor, however a causative relationship has not been proven. For healthy individuals infected with HRV, symptoms are mainly observed from the upper respiratory tract while COPD patients experience more symptoms from the lower respiratory tract. High concentrations of inflammatory cells and molecules have been found in COPD patients and HRV is believed to increase these levels even further. A deeper understanding of the immune mechanisms is required in order to understand the underlying mechanisms of these occurences.

In this master thesis a temporal model of the dynamics between virus and the immune system during a HRV infection was developed. The model was utilized to achieve numerical estimates for parameters governing the mechanisms in the immune system. Through a sensitivity analysis the interplay between different cells in the model was examined. The reliability of the parameter estimates were evaluated through an identifiability analysis.

The model was able to capture the dynamics of virus and the majority of the mechanisms included from the immune system. The sensitivity analysis proved that the outcome of the infection was highly sensitive for changes of the parameters governing the early immune response, production and removal of virus. Lastly the identifiability analysis showed that the model and available data were sufficient to achieve reliable parameter estimates.

Combined with another model that takes the spatial effects into account this model could be used to simulate the infection and immune dynamics in the human lung. With such a model hypothesis regarding the differences in viral occurrence between upper and lower respiratory tract could be tested.

Acknowledgements

This master thesis has been performed during the spring semester of 2018 at the Center for Systems Biology Dresden (CSBD) which is part of the Max Planck Institute of Cell Biology and Genetics (MPI-CBG) in Dresden, Germany. The project has been in collaboration with AstraZeneca in Gothenburg, Sweden. There are some people I would like to thank for their help in this project.

Firstly I wish to thank Ivo Sbalzarini, my supervisor at CSBD for all his advises and support during the project. I would also like to thank Hoda Sharifian and Chris Mccrae at AstraZeneca for their advises and for always putting up on having meetings to discuss even the smallest problems of mine.

Furthermore I would like to thank my supervisors at Lund University Anders Brodin, Department of Biology, and Tobias Ambjörnsson, Astronomy and Theoretical Physics, for their valuable advises and guidance in this project.

I also want to thank my colleagues in the MOSAIC-group for making my time in Dresden memorable and for always taking time to share their expertise and give answer to my questions. Last but not least I wish to thank my family and friends for your limitless support of everything I do.

Dresden, August 2018

Mikaela Giegold

Contents

Chapter 1

Introduction

1.1 Background

Chronic obstructive pulmonary disease(COPD) is an expanding epidemic with global prevalence. With an aging population and increased levels of air pollution the future spread of the disease is expected to expand even further. COPD is a chronic disease and patients can live with their symptoms for many years. Although exacerbations, sudden worsening of the symptom states, can occur often and in their most severe form, lead to death. The exacerbations are associated with a loss in lung function, impaired quality of life as well as enormous health care costs [1]. The latest research shows that viral infections cause the majority of these exacerbations. Therefore, developing drugs with antiviral properties can potentially decrease morbidity and improve patients quality of life. However, the exact mechanism by which virus trigger exacerbations is poorly understood and the movement towards an antiviral drug have been made even more difficult by clinical results from different studies showing contradictory results.

Infection of respiratory viruses, such as Human Rhinoviruses(HRV) was previously thought to be relatively benign illnesses, mainly effecting the upper respiratory tract. However, experimental data suggest that the infection can spread from the upper to the lower tract and that HRV could be linked with COPD exacerbations [2]. Although the detection rates vary and viruses are found in stable COPD patients as well. Therefore a causal relationship between HRV infections and exacerbations in patients with COPD have not yet been made [1].

Patients with COPD have an immune response that is constantly elevated with levels of inflammatory cells that are higher compared to healthy individuals. Additionally, HRV is a pathogen that, even in healthy subjects, trigger the immune response in such a way that the cold symptoms that appear after an infection is considered to be a result from the inflammatory response and not from the virus it-

self [3]. Therefore, by investigating the dynamics of HRV and the immune system interactions during an infection one can learn about the pathogenesis of exacerbations caused by HRV.

1.2 Project

This thesis has been part of a bigger project held in collaboration between CSBD and AstraZeneca in Gothenburg, Sweden. It has been shown in earlier studies that HRV function as a trigger for exacerbations in COPD patients but the underlying dynamics are not yet known. The goal of the bigger project is to deepen the knowledge about these mechanisms by developing a spatiotemporal model that can be used to simulate the virus and the immune dynamics. In parallel with the work presented in this thesis report another master thesis student has worked on developing a spatial model of the human lung with the aim to simulate the viral spread without a counteracting immune system. Eventually the immune system would have to be added to the spatial model but before such extensions can be made it is advantageous to outline which reactions that are likely to occur and which cells and molecules that are going to interact with the virus in the specific scenario of a COPD exacerbation caused by respiratory virus infection.

1.2.1 Aim

The aim of the project has been to develop a model of virus and immune dynamics during a HRV infection and by investigating the dynamics and interactions learn about the pathogenesis of exacerbations caused by HRV.

1.2.2 Objective

The thesis project was divided into the following three sections:

1. A **model** was developed and used to achieve numerical estimates on parameters that govern the mechanisms in the model

2. A **sensitivity analysis** was performed of the model to observe how variations of different parameters effected the model dynamics

3. An **identifiability analysis** was performed in order to explore if the model and available clinical data were sufficient to describe the dynamics and achieve reliable parameter estimates

Chapter 2

Theory

This section presents the theory about the project. Initially the medical conditions related to COPD are outlined in section 2.1 followed by what is known about HRV(section 2.2) and the pathogenesis in healthy subjects(2.2.1). As aforementioned, research has shown contradictory results of the pathogenesis of HRV in patients with COPD. Some of these results are outlined in section 2.2.2. Finally some modelling approaches are presented in section 2.3.

2.1 Chronic Obstructive Pulmonary Disease

Chronic Obstructive Pulmonary Disease (COPD) is a degenerative disease effecting the respiratory system. It has been shown to have a causal relationship with tobacco smoking but pollution and overexposure to other micro particles may also play a role in the progression of the disease. The disease is characterized by airflow obstruction, chronic cough and sputum overproduction and many COPD patients experience a limitation in performing daily life activities due to shortness of breath or fatigue [4]. Chronic Obstructive Pulmonary Disease is often used as an umbrella-term for the conditions Chronic Bronchitis and Emphysema and in some cases these two are even referred to as subtypes of COPD [5].

Chronic Bronchitis (CB) is associated with an increased production of mucus, also called hypersecretion, as a response to inflammation in the epithelium of the airway walls. The inflammation is a response to an elevated immune system triggered by chronic irritation from gases and particles. Normally mucus clearance occurs naturally as the rhythmic movement of the celia, covering the epithelium, shovels the mucus up to the oral cavity. Nevertheless, in COPD patients the celiary function is often impaired leading to decreased elimination of mucus. As a result the overproduction of mucus in combination with ciliary dysfunction leads to chronic cough. [6]

The other condition of COPD, Emphysema, is an illness that causes shortness of breath as a result of impaired alveoli, the smallest compartments of the lungs where the gas exchange takes place. The modern view of Emphysema is that chronic airway inflammation causes the alveolar destruction and that smoking further contributes to the inflammation. When the body is in a state of inflammation the levels of inflammatory cells are locally elevated. These cells secrete proteases which are chemicals that can destroy the walls and the elastic fibres of the alveoli, see figure 2.1 [7]. Some of the inflammatory cells, like the macrophages exist naturally in the alveoli and hence a baseline production of proteases also exists. In a healthy lung the alveoli themselves produce antiproteases to repress the amount of protease as an attempt to maintain equilibrium. However, in the emphysematous lung this production in impaired, leading to an overproduction of protease and an ongoing destruction of tissue. Exposure to toxins from smoking and pollution will further induce the inflammatory response in the sense that it triggers secretion of other inflammatory chemicals, so-kalled cytokines and chemokines.

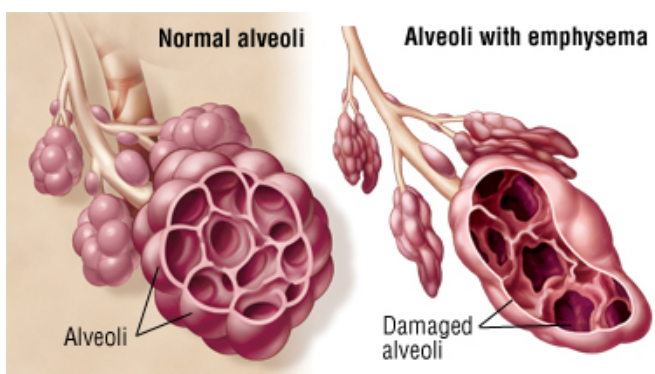

Figure 2.1: An example of normal alveoli and alveoli with emphysema. In patients with emphysema a gradual degradation of the small airways may cause collapse of the alveolar walls. [8]

The elastic fibers in the walls of the alveoli and bronchioles allow recoiling to occur during inhalation and exhalation of gases. In the emhysematous lung the inhalation has to be done with force, due to a decrease in elasticity in the small airways. The forced inhalation results in a narrowing of the bronchioles which in combination with the loss of elastic fibers also makes it hard for the patients to exhale.

2.2 Human Rhinovirus as a pathogen

The presence of respiratory viruses such as Human Rhinovirus(HRV) is often associated with COPD exacerbations. However it has also been recognized as a lower respiratory pathogen in patients with asthma, infants, elderly patients, and immunocompromised hosts. There are currently no approved therapies for prevention or treatment of HRV and the major support that patients can be given are symptom relieving products [2]. It is known that the magnitude of the antibody response during and after an infection depends on the type of pathogen. Some viruses induce a high production of long lived antibodies while the response to other viruses might be only a short lived population of antibodies or none at all. In the case of HRV no such connection has been made. With HRV some patients expressed antibodies, lasting for approximately 2-4 years, while others did not have a production at all [9]. Efforts of producing a vaccine has been hindered by this reason as well as by the large number of serotypes. These serotypes have shown little or no cross-reactivity between each other meaning that an antibody or pharmaceutical that works effectively on one serotype might be useless to another [10].

The pathological effects of HRV in COPD patients have so far been hard to define, mostly because different studies have presented conflicting results. This is probably due to factors such as differences in sampling time, in vivo versus in vitro experiments, differences in time from infection to investigation, effects of treatment and differences with sampling during naturally occurring and induced exacerbations [1]. In the following section the pathogenesis of HRV in healthy subjects will be described followed by what is known to be the differences in the pathogenesis for patients with COPD.

2.2.1 Pathogenesis of HRV in healthy subjects

An HRV infection normally starts by self-inoculation with the virus by hand into the nose or into the eyes [11]. Inoculation of HRV in healthy subjects has shown that the nasopharynx is the most likely area where HRV is initially detected. This is supposedly because the nasopharynx serves as an endpoint for mucus clearance from the nose, paranasal sinuses and middle ear cavities [2]. The nose also has a temperature that is optimal for HRV replication. The targets for HRV are the epithelial cells that constitutes the walls of both the upper and lower respiratory tract and the major receptor in which the virus attaches to the cells is the membrane bound protein ICAM-1. HRV virus has been shown to upregulate the expression of ICAM-1 in order to maximize the infection of epithelial cells [12]. After successfully docking to the receptors the viral RNA enters the cell, where it translates and replicates. New virions are released after 8-10 hours when the in-

fected epithelial cell lyses [3]. Other respiratory viruses, such as influenza, cause a destruction of the neighboring epithelial cells as the infection spreads, but HRV on the other hand has not been associated with such morphological changes of the host tissue [3][2].

A typical immune response to a viral infection consist of both the innate and adaptive immune responses. The innate immunity is the bodys unspecific and initial response that prevents, controls and eliminates the pathogen. The innate response is connected to and initiates the adaptive immune response which is the secondary, specific response that is unique for each pathogen. Cells that are said to be part of the innate response are the dendritic cells, neutrophils, natural killer cells, monocytes(that mature and become macrophages), mast cells, basophils and eosinophils. Among these are mast cells, basophils and eosinophils not associated with HRV infection. There are two types of lymphocytes that are associated with the adaptive immune system. These are B-lymphocytes (B-cells) and T-lymphocytes (T-cells). The T-cells can further be divided into CD8+ that become cytotoxic T-cells (CTLs) and CD4+ that become T helper cells when activated. An overview of the cells in the immune system can be seen in figure 2.2.

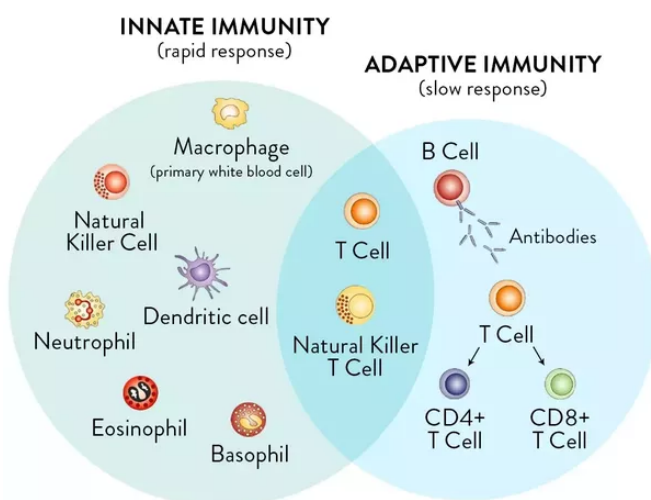

Figure 2.2: The cells of the innate and adaptive immune system. [13]

The Innate response

Following the infection of epithelial cells and within a few hours after inoculation inflammatory mediators, so-kalled cytokines and chemokines, are released by cells in the surrounding tissue. These mediators are the cell's signaling molecules

and they can either be pro or anti inflammatory. The chemokines are a subgroup of cytokines, they are chemotactic cytokines, meaning their major function is to attract other cells by inducing chemotaxis. The first cytokines to be found after HRV infection are type-I interferons (IFN). IFN are produced by infected cells and dendritic cells and the levels peak approximately 1 or 2 days after the peak virus titer [3]. These molecules have gotten their name from their ability of *interfering* with the viral infection. Type-I interferons inhibit the viral replication in both infected and uninfected cells by blocking the receptors on the uninfected cells as well as by interfering with the viral replication in already infected cells [14].

Apart from the type-I interferons multiple other cytokines are produced by the infected cells. Some of these are anti inflammatory with the major function of neutralizing the pro inflammatory cytokines in order to stabilize and calm the inflammation. Others have a chemotactic effect that attract other inflammatory cells. As soon as the chemokine levels increase, inflammatory cells like neutrophils, natural killer cells and macrophages start to migrate towards the area of infection. These cells do not exist in the tissue but circulate in the cardiovascular system until they are recruited from the blood into a site of infection. As the neutrophils, natural killer cells and macrophages arrive they attack the infected cells and in that way they impede with the viral spread.

The Adaptive response

Dendritic cells have a special role in the immunological defence in the sense that they connect the innate immune system with the adaptive. The dendritic cells deliver antigens, which could be part of a pathogen or the pathogen itself, to the lymph nodes and display it to naive CD8+ and CD4+ T-cells. Upon activation the CD8+ T-cells differentiate into Cytotoxic T Lymphocytes (CTLs) and travel to the periphery where they destroy infected cells and virus. When the CD4+ T-cells activate they proliferate into CD4+ helper T-cells with the major function of assisting B lymphocytes with the production of antibodies [14]. The antibodies further assist in the elimination of the virus. The antibody response does however not appear until after 2-5 weeks which implies that the recovery from an infection with HRV, which usually occurs within 7-10 days, must be a result of other components of the immune system [3].

2.2.2 Pathogenesis of HRV in patients with COPD

Active smoking but also exposure to cigarette smoke has shown to upregulate the expression of the epithelial receptor ICAM-1 [15].

The Innate response

Different results have been given regarding the production of type-I IFN by HRV infected COPD cells. In [16] epithelial cells from the lower respiratory tract of COPD patients and controls were infected with HRV in vitro. In this study neither of the groups showed any production of IFN at baseline but increased levels after infection. Additionally, results from [1] in which COPD samples from the lower respiratory tract, cultured ex vivo, of controls and COPD patients indicated on a deficient IFN production by the COPD cells. The deficient IFN production was accompanied by a deficient production of the interferon induced cytokine IP-10.

Results also indicate on an increased basal levels of some pro-inflammatory cytokines. In [16] results showed that epithelial cells, infected in vitro, from the lower respiratory tract of COPD patients expressed more IL-6 and IL-8 than controls. This result was also obtained in [17] where samples were taken from the lower respiratory tract from COPD patients during exacerbations. From the results in [17] the authors made the conclusion that patients with more frequent exacerbations had higher baseline cytokine levels in the lower respiratory tract. Patients with stable COPD had positive correlations between high sputum IL-6 and IL-8 levels and longer history of smoking. These findings could be important for the pathogenesis since positive correlations have been found between virus load and IL-6, IL-8 levels from the lower respiratory tract[1].

In [17] higher levels of IL-8 were also associated with increased cell count of neutrophils. Furthermore the neutrophils from the lower respiratory tract increased significantly over some days in the COPD group but not for controls, as reported in [1].

The Adaptive response

In [18] samples from the lower respiratory tract were taken from controls and COPD patients upon infection with HRV. No differences in any of the T-cell subsets (CD4+ and CD8+) could be found between the groups at baseline. Furthermore they showed that circulating T-cells were recruited from the blood to the lungs in COPD patients during an HRV infection. They also showed that T-cell numbers in the lower respiratory tract correlated with increased virus load and that T-cell clearance was not impaired in COPD patients.

2.3 Different modeling approaches

When it comes to modeling biological systems and particularly the immune system countless different theories and models have previously been proposed. De-

pending on the question that is addressed one model approach might be more beneficial than others. The goal of using a certain model could be to estimate certain parameters, to test competing hypotheses or to study the interplay between a pathogen and a host. Immune responses are part of a complex system that does not only range over a large temporal scale with reactions occurring within milliseconds to days or weeks but also on a large spatial scale including cell to cell distances but also mechanisms that involve the whole body. [19]

Depending if the aim is to study temporal, spatial or both effects this might be important to assess before choosing a modeling method. Furthermore details like what type of relations that should exist between different objects and how the results should be presented might also effect the final choice of method. [20]

The factors that are modeled, which could be cells or molecules, are often described as different compartments or components. The relation between these components are governed by equations that may or may not change the status of one entry or the compartment as a whole. The rates in which these changes occur are determined by unique parameters. [19]

A model that is depending on time is said to be a dynamic model whereas a model that does not take time in consideration is a static model. Time could further on be treated continuously, as is the case in Ordinary Differential Equations (ODEs) and Partially Differential Equations (PDEs), or discrete like in Cellular Automatons (CA). Spatial differences could be modeled continuously, as in PDEs or discrete as in CA or other Agent-Based Models (ABM). Finally, the states of the entries can be modeled continuously, as in PDEs, or discrete, in ABMs [20]. The models that allow states on their entries or agents can further be separated into a group with agents fixed on a grid(such as in CAs) and a group where agents move freely(such as in ABM).

Chapter 3

Methods

3.1 Materials

The experimental data that has been used in this thesis comes from the paper *Experimental Rhinovirus Infection as a Human Model of Chronic Obstructive Pulmonary Disease Exacerbation* [1] by Mallia et al. They present results from an experiment where they infected 13 subjects with COPD and 13 control subjects with a similar smoking history but with normal lung function. After inoculation the concentrations in phlegm from nose and lower airways (sputum) of virus, inflammatory cells and cytokines were measured daily. The data that has been used in this thesis were concentrations of virus in phlegm from the nose(16 time points), concentration of the cytokines IL-6(9 time points) and IL-8(9 time points) in sputum as well as the number of neutrophils(9 time points) in sputum. To each dataset information about standard deviation was also provided. The data was also assessed for normal distribution.

3.2 The Model

In the theory section of this thesis some modeling approaches were presented. The method that was decided upon and utilized further in the thesis have been ordinary differential equations with delays (DDEs) since they allow for computationally simple simulations and easily can be extended or reduced. Furthermore DDEs are functions of time which simplifies the comparison with the clinical data that also was presented over time. The mathematical details of this modeling technique will be described in the following section.

3.2.1 Ordinary Differential Equations

An Ordinary Differential Equation (ODE) is an equation of one or more functions and their derivatives. For ODEs the functions depend only on one independent

variable and if this variable is time the notation becomes y(t). An ODE of n_{th} order can be given on the form

$$y^{(n)}(t) = f(t, y^{(1)}(t), ..., y^{(n-1)}(t)) \tag{3.1}$$

where $y^{(i)}$ is used to denote the i:th derivative of y with respect to t, that is, $y^i = \frac{d^i y}{dt^i}$ for all i=0,1,2...n. An ODE of first order then becomes

$$y^1(t) = \frac{d^1 y}{dt^1} = f(t, y(t)) \tag{3.2}$$

In equation 3.2 the term f is a known function of y and y(t) is called a state variable. ODEs can be used for modeling dynamical systems such as chemical reactions in the cell or the dynamics of an influenza outbreak in a population of a species. The state variables may be called either compartments, species or compounds depending on the field of application. Equation 3.2 describes the dynamics of one such compartment and by integration it gives the time course y(t) of the concentration or quantity of the variable. [21]

Henceforth an initial condition, y_0 and for the model specific parameters, θ, might be added to the equation, as can be seen below.

$$\frac{dy}{dt} = f(t, y(t), \theta) \quad y_0 = y(t_0) \tag{3.3}$$

So far, the left side of equation 3.3 only describes the dynamics of one particular variable. In order to include more species the model can be extended to form a system of m differential equations.

$$\begin{pmatrix} \frac{dy_1}{dt} \\ \frac{dy_2}{dt} \\ \vdots \\ \frac{dy_m}{dt} \end{pmatrix} = \begin{pmatrix} f_1(t, y(t), \theta) \\ f_2(t, y(t), \theta) \\ \vdots \\ f_m(t, y(t), \theta) \end{pmatrix} \quad \bar{y_0} = \begin{pmatrix} y_1(t_0) \\ y_2(t_0) \\ \vdots \\ y_m(t_0) \end{pmatrix} \tag{3.4}$$

In equation 3.4 f_i i=1...m are known functions and $y(t)_i = (y_1(t), ..., y_m(t))^T$ is a m-dimensional variable vector for all i=1...m. $\bar{y_0}$ is a m-dimensional vector containing the initial conditions and θ are vectors of unknown parameters. ODEs can be on either linear or non-linear form. The non-linear equations seldomly have exact solutions which emply that solutions only can be found by numerical approximation.

3.2.2 Delayed Differential Equations

The delayed differential equations (DDE) are similar to ordinary differential equations with the exception that they have delays on the state variables. These delays

can either be constant or time-dependent. This implies that the derivatives at the current time step depends on the solutions from the derivatives at previous times. The delays are often associated with the underlying physiological processes, for example the production time for a certain protein or the delay caused by protein transport. The general form of a first order DDE can be seen in equation 3.5. Here the delays are chosen such that $min(\tau_1, \tau_2, ..., \tau_p) > 0$.

$$\frac{dy}{dt} = f(t, y(t), y(t-\tau_1), y(t-\tau_2), ..., y(t-\tau_p))) \tag{3.5}$$

When the delays are introduced in the ODEs this infer that the history of the state variables at previous times has to be taken in consideration. To give an example, in the case with ODEs the rate of change at the initial time point was given by $y(t_0)$. The DDEs require information from the whole interval $[t_0 - \tau, t_0]$ so the rate of change at the initial point becomes $y(t_0 - \tau)$. Similarly, in order to have the rate of change at time points $t_0 + \varepsilon$ one needs to know $y(t_0)$ and $y(t_0 - \tau + \varepsilon)$. The values of a state variable at previous times are stored in a function called a history function.

As with the ODEs the DDEs can also be nonlinear. A majority of these nonlinear equations cannot be solved analytically so instead a numerical approximation has to be done. Many approximation methods exist but a group of widely used methods for solving first order ODEs are the Runge-Kutta methods. The DDE solver of choice in this thesis, `dde23`, developed for MATLAB, utilizes the Runge-Kutta methods in order to solve nonlinear DDEs. The mathematics behind the approximation method for the differential equations is a comprehensive area *per se* and has not been the focus of this thesis to analyze and therefore the details have been omitted.

3.2.3 The Model

Equations

The equations that make up the model presented in this section have been chosen based on the literature review that was done in the beginning of this project as well as in consideration with Hoda Sharifian and Christopher McCrae at AstraZeneca. Since the immune system consists of a diversity of different cells and cytokines, connected through both positive and negative feedback reactions, modeling the system as a whole would be impossible. Instead the results from the literature review were used to decide which cells and cytokines to include as variables in the model. The final choice of cells and cytokines can be seen in table 3.1.

The first three variables are susceptible cells, infected cells and virus. The susceptible cells serve as the target pool for virions to infect and after the virions

Symbol	Definition
S	Susceptible epithelial cells
I	Infected epithelial cells
V	Free virions
F	Free IFN-β
C	Free IL-8
N	Neutrophils
L	Free IL-6
P	Free IP-10
T	CD8+ T-cells
DC	Dendritic cells in epithelial tissue

Table 3.1: Variable definitions.

successfully infect them they become infected cells. The virus variable, V, represents the free virus that exists in the mucus layer. This was decided upon since the clinical data was collected from the phlegm but it is important to mention that a percentage of virions at an area of infection might also be inside the epithelial cells or attached to receptors on epithelial cells, dendritic cells, in the blood etc. Furthermore the cytokines IFN-β were included since they with their ability to put the infected cells in an anti viral state might have an important role in inhibiting the viral spread. Elevated concentrations of the chemokine IL-8 and neutrophils have been found in some patients with COPD and HRV infections, hence they were added to the model. The chemokines IL-6 and IP-10 function as attractors for CD8+ T-cells. Their concentrations have also been found elevated in patients with COPD during HRV infection. CD8+ T-cells are believed to be important for clearing the infection and they have shown to be present both in COPD patients and in control groups. Lastly dendritic cells were added to the model since they throughout the infection are believed to be a major producer of many important cytokines, as for example IFN-β. The cytokines in this model account only for the free molecules that exist in mucus but as for virus a percentage of these molecules might also be attached to cell surfaces, inside cells, in blood etc.

When the variables were decided upon the system of DDEs was constructed. Equation 3.6 to 3.14 represent evolution of numbers of susceptible cells (S), infected cells (I), free virions (V), IFN-β (F), IL-8 (C), neutrophils (N), IL-6 (L),

IP-10 (P) and CD8+ T-cells (T) respectively.

$$\frac{dS}{dt} = g_S - \beta_1 VS \tag{3.6}$$
$$\frac{dI}{dt} = \beta_1 VS - \beta_2 I - \beta_{12} NI - \beta_{18} TI - \beta_{19} FI \tag{3.7}$$
$$\frac{dV}{dt} = \frac{\beta_3}{(1+\beta_4 F)} I - \beta_7 SV - \delta_V V \tag{3.8}$$
$$\frac{dF}{dt} = \beta_5 I + \beta_{13} DCV - \beta_6 F \tag{3.9}$$
$$\frac{dC}{dt} = g_C + \beta_8 I - \beta_9 C \tag{3.10}$$
$$\frac{dN}{dt} = g_N + \beta_{10} C[t-\tau_1] - \beta_{11} N \tag{3.11}$$
$$\frac{dL}{dt} = g_L + \beta_{14} I[t-\tau_2] - \beta_9 L \tag{3.12}$$
$$\frac{dP}{dt} = \beta_{15} F[t-\tau_3] - \beta_9 P \tag{3.13}$$
$$\frac{dT}{dt} = \beta_{16} L + \beta_{17} P - \delta_T T \tag{3.14}$$

Susceptible cells S, in the absence of infection, proliferate with a rate g_s. They are infected by free virus at rate β_1V and converted to infected cells I. Infected cells decay at a rate β_2. The infected cells can also be killed by neutrophils at rate β_{12}N, CD8+ T-cells at rate β_{18}T or die through apoptosis induced by IFN-β at a rate β_{19}F. Free virus is produced by infected cells at a rate β_3I but the production gets inhibited as IFN puts the infected cells in an antiviral state. This is modeled as a saturation term $\frac{1}{(1+\beta_4 F)}$. The free virus is reduced at rate β_7S as they infect the susceptible cells and decay or is removed due to mucus movement at a rate δ_V. IFN-β F is produced by infected cells and dendritic cells, DC, at a rate β_5 and β_{13}DC respectively. IFN-β decay with a rate β_6. In absence of infection, IL-8 (C), remain at equilibrium g_C with a turn over rate of β_9. If virus is present infected cells produce IL-8 at a rate β_8I. Neutrophils remain at equilibrium g_N in absence of infection and turn over at a rate β_{11}. Neutrophils are recruited to the site of infection at a rate of β_{10}C as a response to elevated IL-8 levels. This recruitment is delayed with a constant τ_1. IL-6 (L) remain at equilibrium g_L in absence of infection and decay with a rate β_9. Furthermore IL-6 is produced by infected cells with a rate of β_{14}I but after a delay of τ_2 hours. IP-10 (P) is produced in response to increased IFN-β levels at a rate of β_{15}F and this production is delayed with τ_3 hours. IP-10 decay with a rate of β_9. CD8+ T-cells are recruited from the periphery at a rate of β_{16}L from IL-6 and β_{17}P from IP-10. They die at a rate δ_T.

For simplicity the number of dendritic cells(DC) are defined as constant. These cells both exist in the tissue and migrate to the area of infection. While at the site of infection they mature and some gets activated and continue to the lymph nodes where they participate in the activation of antigen specific T-cells. Including the dynamics of the DC population would increase the complexity of the model, possibly without improving the accuracy of the results. DCs count as an important producer of IFN so excluding them is not an option. By defining the DCs as constant it is assumed that IFN is produced by those DCs that exist and remain in the tissue.

Systems of ODEs are often supported by a graphical model to make the equations easier to interpret for the reader. Such a model can be seen in figure 3.1.

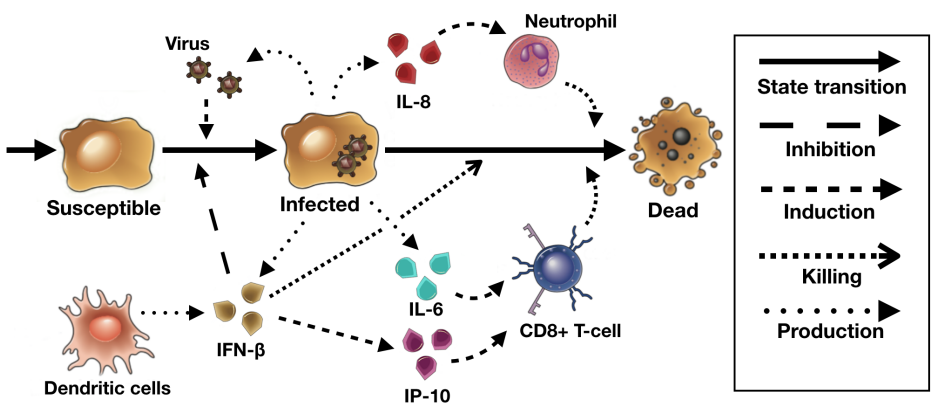

Figure 3.1: Visual representation of the DDE model. Virus infect susceptible cells. The infection is inhibited by IFN-β. IFN-β is produced by infected cells and dendritic cells. IFN-β induce the production of IP-10 and may also induce apoptosis of the infected cells. While in their infected state, the cells produce IL-6. IL-6 together with IP-10 attracts CD8+ T-cells that kills infected cells. The infected cells also produce IL-8. IL-8 attracts neutrophils that also kills infected cells. The model is designed by the author of this thesis with animations from [14].

Initial Conditions

Initial conditions were added to the model based on the data from Mallia et al. if available or from other literature. The susceptible cells were initialized to 10^6 based on results from Mitchel et al. in [22] and the number of initially infected

cells as well as the initial number of IFN-β were both set to zero according to [23]. The initial number of virus was set to 10 which is an estimate about the 1-30 virions needed to infect a new host [10]. The initial concentrations of IL-8 and IL-6 and the quantity of neutrophils were taken from the data provided in Mallia et al. This was done by taking the concentrations measured at time t = 0, or baseline as they refer to it, and use these values as initial conditions. The initial concentration of IP-10 was set to zero since only limited data on this cytokine could be found. The number of CD8+ T-cells were initialized as zero since these cells do not exist in the tissue naturally but arrive during an infection. Furthermore the model was initialized with 1000 DCs which is an approximation made from the assumption of one DC per thousand epithelial cells [10]. The initial conditions with their respective references can be seen in table 3.2.

Symbol	Value	Unit	Reference
S_0 (Susceptible cells)	1000000	cells	[22]
I_0 (Infected cells)	0	cells	[23]
V_0 (Virus)	10	copies/ml	[10]
F_0 (IFN-β)	0	molecules	[23]
C_0 (IL-8)	174	pg/ml	[1]
N_0 (Neutrophils)	103	cells	[1]
L_0 (IL-6)	20	pg/ml	[1]
P_0 (IP-10)	0	pg/ml	-
T_0 (CD8+ T-cells)	0	pg/ml	-
DC (Dendritic cells)	1000	cells	[10]

Table 3.2: Initial conditions for equation 3.6 to 3.14.

3.2.4 Optimization procedure

In order to obtain values for the unknown parameters, such as production rate constants and decay rates, the system of equations, (3.6) to (3.14), was fitted to the virus data from Mallia et al. This was done using the optimization procedure *weighted least squares*. The aim of an optimization through fitting is to find the parameters that yield the best fit of the equations to the data. In order do evaluate the agreement of predictions and data the goodness of the fit is calculated by an objective function that can be of different type depending on the optimization routine. The objective function utilized in this thesis was the weighted sum of squares(WSS) between the fit and the data.

$$WSS = \sum_i \left(\frac{f(x_i, \theta) - x_{obs,i}}{\sigma_i} \right)^2 \tag{3.15}$$

In equation 3.15 the term $f(x_i, \theta)$ represents the output from the nonlinear DDEs with the parameter set θ. $x_{obs,i}$ represents the observed data and i=1...N where N is the number of samples. The differences between predictions and observations are weighted with the standard deviations, σ_i, to each sample. The aim is then to find the parameters that minimize the objective function and hence finds the solution to equation 3.16.

$$\min_{\theta}\left[WSS\right] = \min_{\theta}\sum_{i}\left(\frac{f(x_i,\theta)-x_{obs,i}}{\sigma_i}\right)^2 \tag{3.16}$$

The numerical procedure of the optimization was implemented using the function `lsqcurvefit` in Matlab R2017b. The function was used with default settings.

The fitting was proceeded on data from Mallia et al. The data sets of virus collected from the upper respiratory tract as well as IL-6, IL-8 and neutrophils from the lower respiratory tract was utilized in the fitting procedure.

A total of 25 parameters were fitted in the optimization procedure but since the available data was limited the parameters had to be divided into smaller sets and optimization performed on each subset. Hence the optimization carried out was a local optimization. The parameters were divided into four subsets containing 6, 6, 6 and 7 parameters respectively. This gave 2-3 data points for each parameter which is about the least possible in order to get a good fit according to the recommendation given in [24].

In order to limit the parameter search space for the `lsqcurvefit` function boundaries were added on all parameters that were fitted. For some parameters reference ranges were found in literature and for others the boundaries had to be determined by the author. All the parameters that were fitted together with their units and reference ranges, if available, can be seen in table 3.3.

When a model is nonlinear and fitted to a dataset with few samples the landscape of possible solutions obtained when searching for a best fit in a multiple parameter space might exhibit many local optima [25]. The search for a global optimum could be enhanced by increasing the number of steps but often this is not enough. To ensure that the solution found by the optimization algorithm was indeed the best fit a multistart approach was implemented together with the `lsqcurvefit` algorithm. This means that the fitting was performed multiple times, each from a new starting position i.e with a new set of starting parameters. The starting parameters were chosen randomly by the algorithm within the boundaries for each parameter. A number of 25 multistarts were used.

Parameter	Unit	Param. ranges from literature	Ref
β_1	$(copies/ml)^{-1}(day)^{-1}$	[6e-06, 1.7e-04]	[26]
β_2	$(day)^{-1}$	[2.5e-01, 4.0]	[27]
β_3	$(copies/ml)(day)^{-1}$	-	-
β_4	dim.less	[1e-08, 3.4e-03]	[23]
β_5	$(molecules/cell)(day)^{-1}$	-	-
β_6	$(day)^{-1}$	[1, 80]	[27]
β_7	$(day)^{-1}(cell)^{-1}$	-	-
β_8	(pg/ml)$(cell)^{-1}(day)^{-1}$	[3.8e-03, 1.5e-01]	[28]
β_9	$(day)^{-1}$	[1, 80]	[27]
β_{10}	$(Neutrophils/day)(pg/ml)^{-1}$	-	-
β_{11}	$(day)^{-1}$	[1e-01, 2.4]	[28]
β_{12}	$(Neutrophil)^{-1}(day)^{-1}$	[2.5e-06, 1e-03]	[28]
β_{13}	$(molecules/cell)(day)^{-1}(pg/ml)^{-1}$	-	-
β_{14}	$(pg/ml)(cell)^{-1}(day)^{-1}$	[3.8e-03, 1.5e-01]	[28]
β_{15}	$(day)^{-1}$	[3.8e-03, 1.5e-01]	[28]
β_{16}	$(cells/day)(ml/pg)^{-1}$	-	-
β_{17}	$(cells/day)(ml/pg)^{-1}$	-	-
β_{18}	$(day)^{-1}(cell)^{-1}$	[1e-06, 1e-05]	[10]
β_{19}	$(molecules)^{-1}(day)^{-1}$	-	-
δ_V	$(day)^{-1}$	[3.1, 8.7]	[26]
δ_T	$(day)^{-1}$	[1e-02, 1e-01]	[29]
g_S	$(day)^{-1}$	-	-
g_C	$(pg/ml)(day)^{-1}$	-	-
g_N	(cells/day)	-	-
g_L	$(pg/ml)(day)^{-1}$	-	-
τ_1	(h)	peak approx. 9-12 dpi.	[1]
τ_2	(h)	peak approx. 3 dpi.	[30]
τ_3	(h)	peak approx. 2-3 dpi.	[23]

Table 3.3: Parameters included in the DDE model. Estimates for parameter β_1 to g_L were found by fitting the differential equations to virus data or by manually changing the parameters in order to find a good fit. Estimates for τ_1 to τ_3 were found by manually changing their respective values. Reference ranges for some of the parameters were found in literature and used as boundaries in the optimization routine. dpi. = days post infection.

3.3 Sensitivity analysis

The sensitivity analysis serves two purposes. The first one is to examine how the model behaviour changes as a single parameter is varied. Secondly, it allows to see which of the parameters that has a large impact on model behaviour [23]. In this thesis the sensitivity analysis was performed according to the One Factor At

a Time (OFAT) approach. As the name OFAT suggests this analysis is performed by varying the value of one parameter at a time while holding the others fixed. From the system of equations (3.6) to (3.14) 25 parameters were included in the sensitivity analysis. The parameters that were excluded from the analysis were the time constants, τ_1 to τ_3, governing the delay of the equations. The OFAT analysis is computationally efficient and requires only n+1 model runs for a n-dimensional parameter space which made it a suitable choice for this application since the model contains relatively many parameters.

3.3.1 Virus sensitivity

In the first part of the sensitivity analysis the changes in viral load was observed while the parameters were varied. This was done by first fitting the DDE model, equation (3.6) to (3.14), to data from Mallia et al. in order to obtain estimates for parameter β_1 to g_L. These values were used as baseline values for the parameters.

Thereafter each of the parameters were varied one at a time in steps of four between 0.5, 0.75, 1.5 and 2 of their baseline values. For each step the DDEs were solved and a new trajectory for the virus concentration was achieved yielding four new trajectories for each parameter. For each step the l_2-norm, equation 3.17, between the trajectory obtained with the baseline parameter and the trajectory obtained with the modified parameter was calculated.

$$l_2 = \|x - x_{default}\|_2 = \sqrt{\sum_i \left(x_i - x_{default,i}\right)^2} \tag{3.17}$$

In equation (3.17) x_i is the vector obtained with the modified parameter and $x_{default,i}$ the vector obtained with the baseline parameters.

The output of the l_2-norm has the same unit as the data that it is applied on. Hence the results from the virus sensitivity analysis was given in $log_{10}(copies/ml)$ which is the unit used for virus in the paper from Mallia et al. In order to make the outputs from the l_2-norm easier to interpret and compare with each other they were normalized with the virus peak value from the trajectory obtained with the baseline parameters as seen in equation (3.18).

$$l_{2,normalized} = \frac{l_2}{x_{peak}} \tag{3.18}$$

3.3.2 Other variables sensitivity

Since it was of interest in this project to model not only the virus dynamics but also the other variables in a biologically meaningful way the sensitivity analysis was extended to investigate how each parameter affected each of the variables in

the DDE model.

The procedure, which was similar to the one exploring virus sensitivity, started by fitting the DDE model to the virus data from Mallia et al. to get a set of baseline parameter values as well as baseline trajectories for each of the variables. From their baseline values the parameters were varied one at a time in steps of four between 0.5, 0.75, 1.5 and 2 times their initial values. For each step the DDEs were solved in order to achieve four new trajectories for each variable. The l_2-norm was then calculated between the baseline trajectory and the trajectories obtained with the modified parameters. This process was repeated for all the parameters.

The outputs from the l_2-norm was normalized by the peak value of their respective variable. The parameters were then classified into sensitive, partly sensitive and stable depending on the size of the l_2-norm.

3.3.3 Use of the model to test two hypotheses

If a model is able to describe the dynamics it is designed for it can be used to test different hypotheses that have been postulated about the behaviour of the system. In this thesis this was done by trying to replicate two results that have been obtained during clinical experimentation. This was done by changing some parameter values, solving the system of DDEs and observing the changes of the trajectories.

Elevated neutrophil levels
Mallia et al. showed in [1] that the number of neutrophils are higher in COPD patients than in controls during an infection. Therefore the parameters governing baseline growth of IL-8 (g_C), baseline growth of neutrophils (g_N) and the neutrophil migration rate (β_{10}) were increased while observing the changes of the neutrophil trajectory. The initial condition of neutrophils was also changed from 103 cells, which was the baseline value for controls, to 127 cells which was the baseline value for COPD patients.

Impaired production of IFN-β
The results from Mallia et al. also suggested that a deficient production of IFN-β may contribute to increased susceptibility to virus infection in COPD subjects. To test this hypothesis the parameters governing IFN-β production induced by infected cells (β_5) and by dendritic cells (β_{13}) were decreased while changes of the virus trajectory was observed.

3.4 Identifiability analysis

A critical challenge with biological models is that they tend to have a lot of parameters whose values usually are unknown for the modeler and hence have to be estimated. It may also be that the available experimental data is only from one or a few species in the model. If this is the case then the amount and quality of data might not be sufficient to estimate the model parameters unambiguously [31]. It could also be that the model itself is not appropriately designed to describe the dynamics. In any of these scenarios it could be that the parameters are *non-identifiable*. It might however still be possible to find an estimate for a non-identifiable parameter but the achieved value will not be uniquely identified and may not be reliable. An identifiability analysis was performed on parameter β_1 to g_L to determine the reliability of their estimates.

A number of definitions and methods of determining identifiability exist in the literature. The method that has been utilized in this thesis is the one presented by Raue et al. [31] in which they focus on distinguishing structural and practical non-identifiable parameters from the ones being fully identifiable. This is done by utilizing the profile likelihood (PL) to search for non-identifiabilities. The identifiability analysis was performed using the virus data from upper respiratory tract from Mallia et al.

The approach will be presented by first introducing the connection between weighted least squares (WLS) and maximum likelihood (ML) followed by the connection between maximum likelihood and profile likelihood. Lastly the fundamentals for calculating confidence intervals by using the profile likelihood will be given.

Connection between weighted least squares, maximum likelihood and profile likelihood

When a model is fitted to data the agreement of the fit to the experimental data is often measured using an objective function, like the weighted least squares introduced in the model section of this thesis and presented again below.

$$WSS = \sum_i \left(\frac{x_i - f(x_i, \theta)}{\sigma_i} \right)^2 \tag{3.19}$$

With the weighted least square method the objective function, WSS, is minimized in order to find the set of parameters θ that yield the best fit to the data, x_i. In equation 3.19 the vector of observations can also be written $x_i = y_i + \varepsilon_i$ where y_i are the true measurement values and ε_i are the noise that is added to each measurement. In this project the data from Mallia et al. was assumed to have

normally distributed observational noise with zero mean and known variance, i.e

$$\varepsilon_i \sim \mathcal{N}(0, \sigma_i^2)\,.$$

The maximum likelihood can also be used for parameter estimation and the method are in those cases referred to as maximum likelihood estimation (MLE). The likelihood, $L(\theta|x_1..x_N)$, gives the likelihood of observing a desired set of parameters θ given a certain set of data, $x_1..x_N$. The higher the likelihood becomes the higher are the chances to obtain the desired parameters and therefore the likelihood function is maximized.

As previously stated the observational noise in the measurements from Mallia et al. were assumed to have a gaussian distribution. This implies that the probability of observing a single data point x_i is given by the probability density function (PDF), equation 3.20, of the Gaussian distribution. The PDF should not be confused with the output of the DDEs and is therefore denoted with the subscript PDF.

$$f(x_i, \theta)_{PDF} = \frac{1}{\sqrt{2\pi\sigma_i^2}} exp\left(-\frac{(x_i - \mu_i)^2}{2\sigma_i^2}\right) \tag{3.20}$$

In equation 3.20 the PDF of a single data point x_i is given and σ_i and μ_i denotes the standard deviation and mean. Since the data set utilized in this thesis does not consist of only one sample but a vector of samples the joint PDF of these samples was required. If the data is discrete the joint PDF of a vector of independent observations is equal to the product of the PDFs for each sample, equation 3.21.

$$f(x_1...x_N, \theta)_{PDF} = f(x_1, \theta)_{PDF}...f(x_N, \theta)_{PDF} = \prod_{i=1}^{N} f(x_i, \theta)_{PDF} \tag{3.21}$$

The likelihood function is by definition the joint PDF of the observations and can hence be written as in equation 3.22

$$L(\theta|x_1...x_N) = \prod_{i=1}^{N} f(x_i, \theta)_{PDF} = \prod_{i=1}^{N} \frac{1}{\sqrt{(2\pi\sigma_i^2)^n}} exp\left(-\frac{(x_i - \mu_i)^2}{2\sigma_i^2}\right) \tag{3.22}$$

To recall from previously the goal in MLE is to maximize the likelihood in order to find the optimal parameters. This is achieved by taking the derivative $\frac{\partial L}{\partial \theta}$ of equation 3.22, set it equal to zero and solve for θ. In this process equation 3.22 is often logaritmized on both sides in order to make the computations easier. Since the logarithm is an increasing function maximizing it will be equal to maximizing

the non logaritmized function. It yields:

$$log(L(\theta|x_1...x_N)) = -\frac{1}{2}\sum_{i=1}^{N}\frac{(x_i-\mu_i)^2}{\sigma^2}log\left(\frac{1}{\sqrt{(2\pi\sigma_i^2)^n}}\right) \tag{3.23}$$

The term $log(\frac{1}{\sqrt{(2\pi\sigma_i^2)^n}})$ does not effect the estimate on θ and can therefore be removed when taking the derivative of equation 3.23. Furthermore suppose that the mean, μ, is given as a function of x that is depending on θ. This makes it equivalent to the output from the DDEs. The final result after taking the logaritm and derivative can be seen in equation 3.24.

$$\frac{\partial}{\partial\theta}\left(log(L(\theta|x_1...x_N))\right) = -\frac{1}{2}\sum_{i=1}^{N}\frac{(x_i-f(x_i,\theta))^2}{\sigma_i^2} \tag{3.24}$$

The next step in the process of finding the optimal parameters would be to set equation 3.24 to zero and solve for θ. Although this will not be done here since the purpose of the above calculations were to show the connection between weighted least squares and maximum likelihood. Finally the connection between the log likelihood and weighted least squares optimizer can be summarized as

$$WSS = constant - 2log(L(\theta|x_1...x_N)) \tag{3.25}$$

which imply that for normally distributed observational noise minimizing the weighted least square is equal to maximizing the log likelihood. [31]

Profile likelihood

The likelihood can also be used if the aim is to estimate only one of the total number of parameters and it is then called the profile likelihood. This can be done if the parameters that are not of interest, the nuisance parameters, can be expressed as a function of the desired parameter. Then the likelihood becomes a function of the single parameter, θ_i, when maximized over all the other parameters $\theta_{j\neq i}$. [32]

$$PL(\theta_i) = \max_{\theta_{j\neq i}}(log\ L(\theta_j)) \tag{3.26}$$

Profile likelihood confidence intervals

By exploring the profile likelihood, Raue et al. postulate that it is possible to detect structural and practical non-identifiabilities. This is achieved by determining likelihood based confidence intervals. In [31] the following definition of a CI is given:

> *A confidence interval $[\sigma_i^-,\sigma_i^+]$ of a parameter estimate θ_i to a confidence level α signifies that the true value θ_i^* is located within this interval with probability α.*

This implies that even though an estimate has successfully been found for a parameter its true value can only be guaranteed to lay within the confidence interval with a certain probability for which the uncertainties are described by the confidence intervals.

Likelihood ratio test

The idea of the PL based confidence intervals is to invert a likelihood ratio test to obtain CIs for the desired parameter. In the likelihood ratio test a null hypothesis and an alternative hypothesis is defined, equation 3.27. The null hypothesis, H_0, is that the parameter of interest, θ, equals a fixed constant value θ_0. The alternative, two-sided hypothesis H_1 is that θ is not equal to this value.

$$\begin{aligned} H_0 &: \theta = \theta_0 \\ H_1 &: \theta \neq \theta_0 \end{aligned} \tag{3.27}$$

The definition of the test ratio is given by

$$2\Big(logL(\theta) - logPL(\theta_0)\Big) \leq \chi^2(\alpha, \mathrm{df}) \tag{3.28}$$

where the term $logL(\theta)$ is the output of the likelihood with the full parameter set and the term $logPL(\theta_0)$ is the output of the likelihood with a reduced number of parameters i.e the profile likelihood. The term $\chi^2(\alpha, \mathrm{df})$ on the right hand side in equation 3.28 denotes the 100(1-α)th percentile of the χ^2 distribution with a degree of freedom df. The χ^2 distribution is used since the left side of equation 3.28 approximates to the χ^2 distribution for large sample sets. If θ_0 fulfills equation 3.28 then the null hypothesis would not be rejected. Hence, a $100(1-\alpha)$ confidence interval for a parameter consists of all possible values of theta for which the null hypothesis would not be rejected at a significance level α.

In the identifiability analysis performed in this thesis 95% confidence intervals were desired. The degree of freedom, df, is often chosen to be 1 which yields confidence intervals that are individual for each parameter. From the table with the χ^2 distribution this gives $\chi^2_{\alpha=0.95,\mathrm{df}=1}$=3.84. Then a 95%-confidence interval for a parameter contains those values of θ for which the left hand side of equation 3.28 does not exceed 3.84. Graphically this can be viewed in figure 3.2. Here the result from the full model is demonstrated by the round black dot and the 95% interval includes all values of θ for which the loglikelihood function drops off by no more than 1.92.

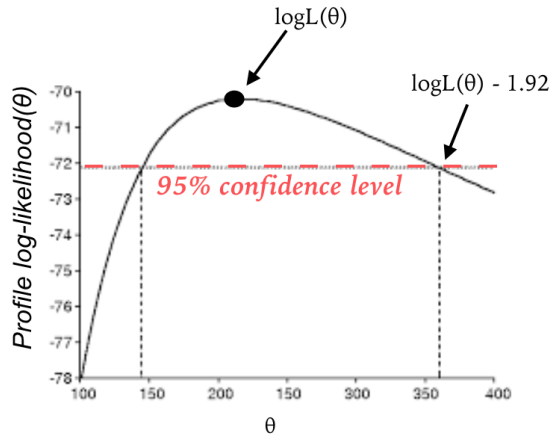

Figure 3.2: A profile likelihood calculated using the likelihood function. The black dot represents the likelihood estimated with the full parameter set. The threshold for the 95% CI is marked by the dashed red line.

As previously shown, for gaussian observational noise the maximum likelihood and profile likelihood is connected as in equation 3.25. By using this relation and substituting the logarithmized likelihood terms in equation 3.28 the test ratio can be written as in equation 3.29 below.

$$2\left(\frac{const.-WSS(\theta)}{2}-\frac{const.-WSS(\theta_0)}{2}\right)\leq\chi^2(\alpha,\mathrm{df})=3.84 \qquad (3.29)$$

After cancelling the constants and re-arranging the terms this equation becomes

$$WSS(\theta_0)-WSS(\theta)\leq 3.84 \qquad (3.30)$$

This relation can be viewed graphically in figure 3.3. Here the result from the full model is denoted by the black asterisk and a 95% interval includes all values of θ for which the error of the weighted least square optimizer does not increase by more than 3.84.

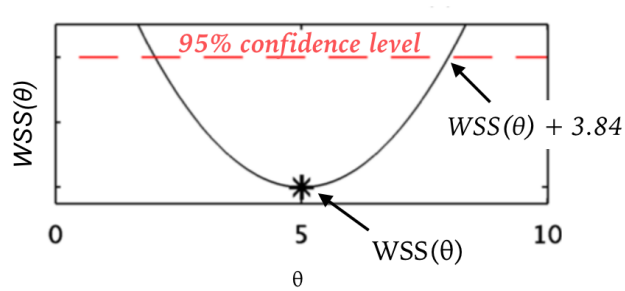

Figure 3.3: A profile likelihood calculated using weighted least squares. The asterisk denote the error from the WLS optimizer calculated with the full parameter set. The threshold for the 95% CI is marked by the dashed red line.

By showing the above relation Raue et al. were able to use the weighted least square to calculate profile likelihoods and determine confidence intervals for a given parameter.

Structural and practical non-identifiabilities

The profile likelihood shown in figure 3.3 exceeds the 95% confidence level on both sides of the estimate achieved with the full model. However this is not always the case and by determining the CIs using the profile likelihoods it is possible to obtain non-identifiabilities.

Graphically a profile likelihood that is completely flat in both directions indicate on a structural non-identifiability. A structurally non-identifiable parameter occurs as a result of a redundant parameterization of the model. Varying such a parameter will not change the trajectories of the variables in the model and will hence keep the WSS on a constant level, the CIs are infinite $[-\infty, \infty]$. A parameter is structurally identifiable only if a unique minimum in the PL exists. An example of the PL for a structurally non-identifiable parameter can be seen in figure 3.4, left panel. In the three plots in figure 3.4 the red line represents $\chi^2_{\alpha=0.95,\mathrm{df}=1}$=3.84. The values of the x-axis where the PL crosses the red line represent the lower and upper boundary of the confidence intervals.

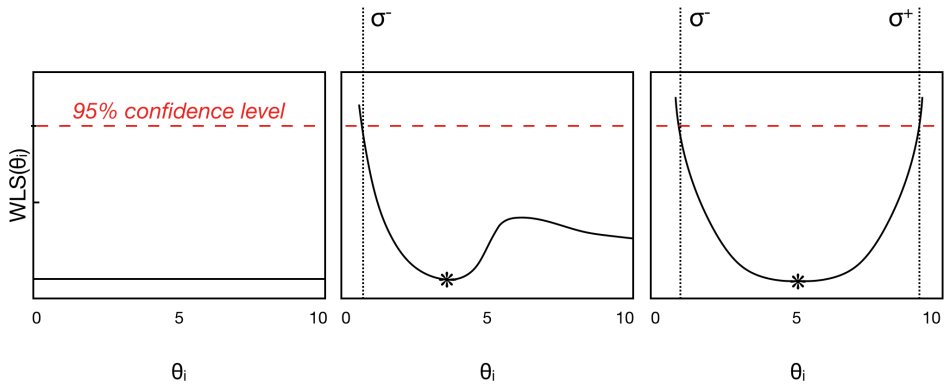

Figure 3.4: Three different outcomes of the profile likelihood. Parameter θ_i is varied in both directions of the value obtained by the full model, indicated by the black asterisk, and the other parameters are re-optimized for each step. The dashed red line marks the threshold $\chi^2_{\alpha=0.95,\mathrm{df}=1}$. The CIs are marked by $[\sigma^-, \sigma^+]$. Left panel: structural non-identifiability, mid panel: practical non-identifiability, right panel: fully identifiable.[33]

A parameter that is structurally identifiable may still be practically non-identifiable. A practically non-identifiable parameter can be recognized with a PL that has a minimum and exceeds the $\chi^2_{\alpha=0.95,\mathrm{df}=1}$ threshold in either increasing or decreasing directions but not in both. This means that one of the CIs is finite while the other is still infinite. The cause is often an insufficient amount of data or data with a low signal to noise ratio. A modification of a practically non-identifiable parameter results in a small change of the trajectory it governs. However it may have a bigger effect on the trajectories of the other species. An example of practical non-identifiability can be seen in the mid panel of figure 3.4.

If the parameter is fully identifiable it has finite CIs and a PL that exceeds the threshold in both directions from the result obtained with the full model. The PL of an identifiable parameter can be seen in the right panel of figure 3.4.

3.4.1 Resolving non-identifiabilities

Estimates from non-identifiable parameters might be spurious and unreliable. However, the results from the identifiability analysis can be used to either plan new experiments or to reduce the model which possibly could resolve some of the non-identifiabilities.

Structural non-identifiability can only be resolved by modifying the design of

the model and not by adding more data. Such a modification of the model could for example be to add more species, provide the model with initial conditions or fix a parameter to a user-defined value that yields the desired outcome. Practical non-identifiablity can in some cases be resolved by adding more data. In such cases the data should preferably be of the species the parameter is governing. Furthermore the parameter can be set to zero. i.e by removing the corresponding reaction from the model. [25]

In this part of the identifiability analysis the data set of IL-8 and IL-6 from Mallia et al. was added so that the DDE model was fitted to virus, IL-8 and IL-6 data simultaneously.

Chapter 4

Results

4.1 The model

The results from the fitting procedure can be seen in figure 4.1 and 4.2. In these figures the data sets from Mallia et al. are presented with their respective error bars. The trajectories that do not have error bars are the results from the DDE model.

Susceptible and infected cells
The upper left panel of figure 4.1 shows the trajectories of the susceptible and infected cell variables. The number of infected cells increase as they are infected by free virus and peak between 4-5 days post infection (dpi.) followed by a decrease. The number of infected cells at day 42, the last day of measurement, is 11.

Virus
In the upper right panel the virus data collected in the upper respiratory tract is shown with error bars and the fitted virus trajectory can be seen in red.

IFN-β
The first response and threat to the virus infection is the increased production of IFN-β, seen in the lower left panel of figure 4.1. These molecules inhibit the viral infection of susceptible cells and is hence responsible for the saturation of the viral increase. The trajectory of IFN-β has the peak load 4-5 dpi.

IL-8
In the lower right panel of figure 4.1 the data of IL-8 from the lower respiratory tract is presented in blue. The red trajectory represents the fit of IL-8 and it has a peak load after 4-5 dpi.

Neutrophils

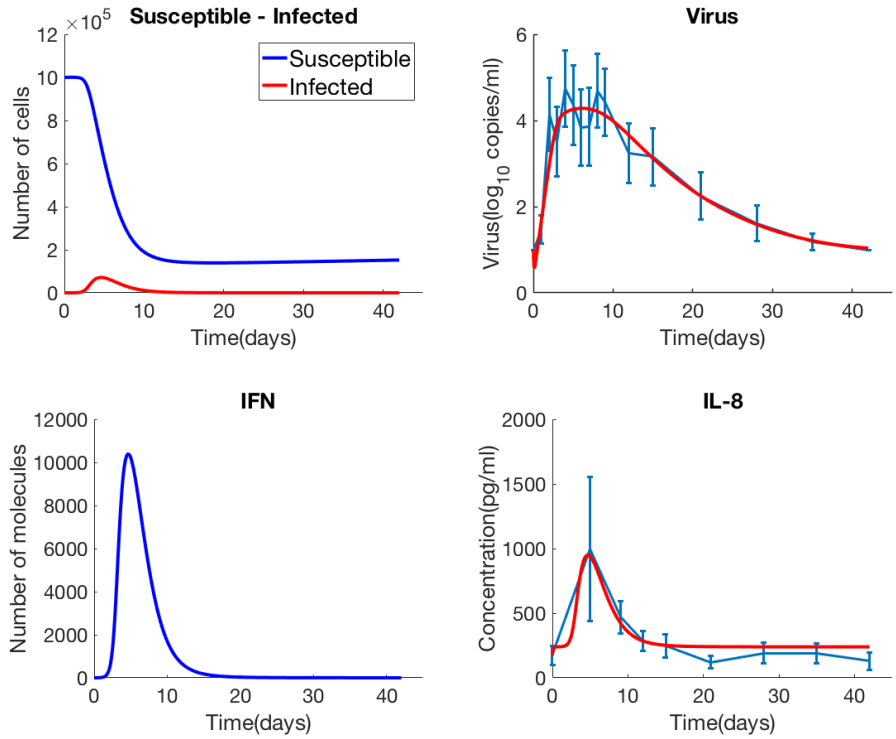

Figure 4.1: Results of fitting the DDE model to the dataset of virus, IL-8, IL-6 and neutrophils. Upper left panel: susceptible and infected cells, upper right panel: virus and virus data from the upper respiratory tract, lower left panel: IFN-β, lower right panel: IL-8 and IL-8 data from the lower respiratory tract.

The neutrophils increase as a response to increased levels of IL-8. In the upper left panel of figure 4.2 data from the lower respiratory tract of neutrophils is presented with error bars. The red trajectory is the fit of neutrophils. It has a peak at 9 dpi.

IL-6

In the upper right panel the fit of IL-6 can be seen in red and the data of IL-6 from the lower respiratory tract is marked by the error bars. The peak concentration of the fit occur 9 dpi.

IP-10

In the lower left panel of figure 4.2 the concentration of IP-10 can be seen. IP-10 is produced as a response to IFN-β production and it has a peak at 6 dpi.

CD8+ T-cells

As a response to IL-6 and IP-10 the CD8+ T-cells migrate to the site of infection. The trajectory of CD8+ T-cells can be seen in the lower right panel of figure 4.2. The peak occurs between 9-11 dpi.

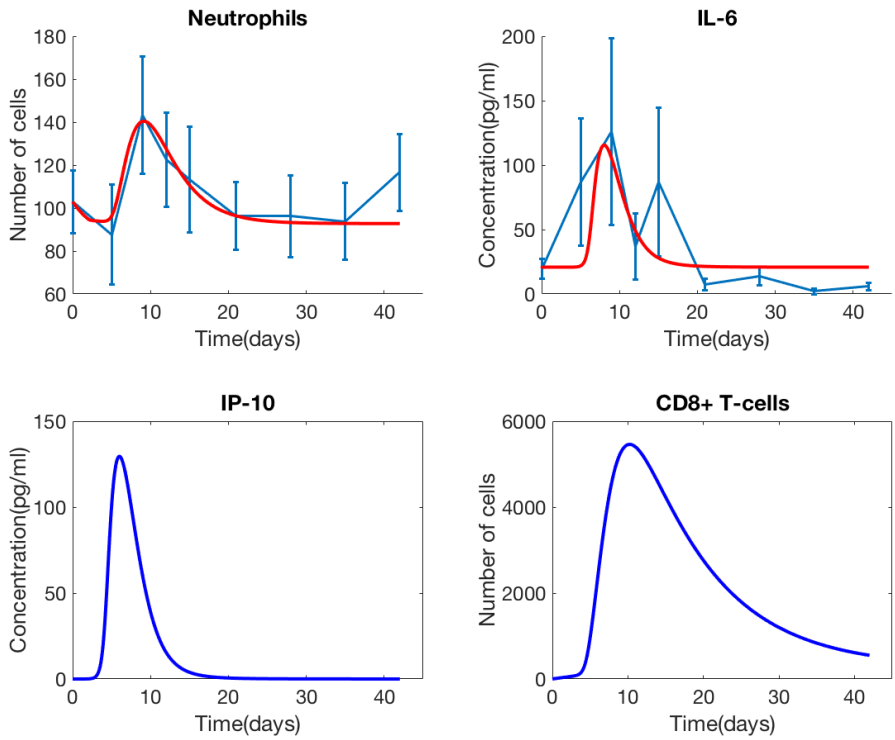

Figure 4.2: Results of fitting the DDE model to the dataset of virus, IL-8, IL-6 and neutrophils. Upper left panel: neutrophils and neutrophil data from the lower respiratory tract, upper right panel: IL-6 and IL-6 data from the lower respiratory tract, lower left panel: IP-10, lower right panel: CD8+ T-cells.

Estimates for the parameters in the DDE model can be seen in table 4.1. The parameter estimates are given with the reference ranges that were found for some of the parameters and used as parameter boundaries in the fitting procedure.

4.2 Sensitivity Analysis

4.2.1 Virus sensitivity

In the first part of the analysis the sensitivity of the model in terms of virus concentration was examined. The parameters were varied independently from 0.5,

Parameter	Estimate	Units	Param. ranges from literature	Ref
β_1	1.4624e-05	$(copies/ml)^{-1}(day)^{-1}$	[6e-06, 1.7e-04]	[26]
β_2	2.240	$(day)^{-1}$	[2.5e-01, 4.0]	[27]
β_3	7.01	$(copies/ml)(day)^{-1}$	-	-
β_4	1.2557e-04	dim.less	[1e-08, 3.4e-03]	[23]
β_5	2.4951	$(molecules/cell)(day)^{-1}$	-	-
β_6	17.0897	$(day)^{-1}$	[1, 80]	[27]
β_7	1.0903e-05	$(day)^{-1}(cell)^{-1}$	-	-
β_8	0.12	$(\text{pg/ml})(cell)^{-1}(day)^{-1}$	[3.8e-03, 1.5e-01]	[28]
β_9	12.02	$(day)^{-1}$	[1, 80]	[27]
β_{10}	0.035	$(Neutrophils/day)(pg/ml)^{-1}$	-	-
β_{11}	0.306	$(day)^{-1}$	[1e-01, 2.4]	[28]
β_{12}	9.9090e-04	$(Neutrophil)^{-1}(day)^{-1}$	[2.5e-06, 1e-03]	[28]
β_{13}	7.9671e-06	$(molecules/cell)(day)^{-1}(pg/ml)^{-1}$	-	-
β_{14}	0.016	$(pg/ml)(cell)^{-1}(day)^{-1}$	[3.8e-03, 1.5e-01]	[28]
β_{15}	0.15	$(day)^{-1}$	[3.8e-03, 1.5e-01]	[28]
β_{16}	1.2857	$(\text{cells/day})(\text{ml/pg})^{-1}$	-	-
β_{17}	12.6389	$(\text{cells/day})(\text{ml/pg})^{-1}$	-	-
β_{18}	8.6322e-05	$(\text{day})^{-1}(\text{cell})^{-1}$	[1e-06, 1e-05]	[10]
β_{19}	0.000003	$(\text{molecules})^{-1}(\text{day})^{-1}$	-	-
δ_V	5	$(\text{day})^{-1}$	[3.1, 8.7]	[26]
δ_T	0.1	$(\text{day})^{-1}$	[1e-02, 1e-01]	[29]
g_S	700	$(\text{day})^{-1}$	-	-
g_C	2.8788e+03	$(\text{pg/ml})(\text{day})^{-1}$	-	-
g_N	20	(cells/day)	-	-
g_L	250	$(\text{pg/ml})(\text{day})^{-1}$	-	-
τ_1	50	(h)	peak approx. 1-2 dpi.	[1]
τ_2	80	(h)	peak approx. 9-12 dpi.	[30]
τ_3	30	(h)	peak approx. 3 dpi.	[23]

Table 4.1: The parameters in the DDE model. Estimated values can be seen with thir respective units and parameter reference ranges, if available, from literature.

0.75, 1.5 and 2 times the initial best fit values according to the OFAT-approach. The model was re-run for each change of parameters and the results were compared between the new and old trajectory using the l_2-norm. The output from the norm was normalized with the peak value of the default trajectory to make the results easier to compare. The l_2-norms for each step and parameter are presented in table 4.2. As a complement the trajectories of each parameter change were plotted and the result can be seen in Appendix B.

Large values of the l_2-norms indicate a significant change of the virus trajectory meaning that the virus load is sensitive for changes of this parameter. The parameters β_1 to β_7 as well as δ_V all have large values indicating that they are sensitive parameters. This is supported by the trajectories of these parameters seen in figure B.1 and B.2.

Parameter	Parameter change			
	0.5	0.75	1.5	2
β_1, Infection rate of susceptible cells	2.3775	1.2281	1.6870	2.5521
β_2, Decay rate of infected cells	1.1187	0.5411	0.9545	1.7661
β_3, Virus production rate	2.2613	1.3013	2.6191	4.9249
β_4, Inhibition of viral production by IFN	1.8954	0.7232	0.8298	1.2646
β_5, Production of IFN by infected cells	1.9746	0.7427	0.8364	1.2695
β_6, Decay rate of IFN	1.2654	0.6188	1.0793	1.9775
β_7, Infection rate of susceptible cells	1.9170	0.9080	1.3303	2.0404
β_8, Production rate of IL-8	0.0177	0.0088	0.0175	0.0348
β_9, Decay rate of IL-8, IL-6 and IP-10	0.3410	0.1226	0.1374	0.2126
β_{10}, Migration rate of neutrophils	0.0250	0.0124	0.0245	0.0485
β_{11}, Decay rate of neutrophils	0.0564	0.0226	0.0276	0.0437
β_{12}, Kill rate by neutrophils	0.0513	0.0255	0.0501	0.0992
β_{13}, Production rate of IFN by DCs	0.0012	6.17e-04	0.0012	0.0025
β_{14}, Production rate of IL-6	0.0098	0.0050	0.0096	0.0192
β_{15}, Production rate of IP-10	0.1694	0.0817	0.1485	0.2851
β_{16}, Migration rate of T-cells by IL-6	0.0132	0.0066	0.0130	0.0259
β_{17}, Migration rate of T-cells by IP-10	0.1694	0.0817	0.1484	0.2851
β_{18}, Kill rate by T-cells	0.1837	0.0882	0.1589	0.3034
β_{19}, Apoptosis rate induced by IFN	0.0113	0.0056	0.0111	0.0221
δ_V, Virus decay rate	1.8551	0.6755	0.7912	1.2730
δ_T, T-cell decay rate	0.0585	0.0282	0.0494	0.0905
g_S, Baseline growth of susceptible cells	0.0109	0.0055	0.0119	0.0266
g_C, Baseline growth of IL-8	0.0087	0.0044	0.0087	0.0173
g_N, Baseline growth of neutrophils	0.0226	0.0113	0.0225	0.0449
g_L, Baseline growth of IL-6	0.049	0.0024	0.0047	0.0095

Table 4.2: Normalized l_2-norm values between virus default trajectory and the trajectories obtained with each modified parameter. Each parameter was modified to 0.5, 0.75, 1.5 and 2 times the default value, the system was resolved and the l_2-norm was calculated between the default curve and the ones obtained with the changed parameters. The output was then normalized with the peak concentration of the default virus trajectory.

4.2.2 Sensitivity of the other variables

The extended sensitivity analysis was done by using the OFAT-approach while observing the changes of the other variables as the parameters were modified. For each parameter four l_2-norm values were achieved per variable yielding in a table

like the one presented below for β_1. The result of the other parameters can be seen in Appendix A.

Parameter β_1. l_2-norms						
Parameter change	IFN	IL-8	Neutrophils	IL-6	IP-10	T-cells
0.5	1.8857	1.4017	0.7988	1.5220	1.8578	2.6650
0.75	1.1918	0.8859	0.4003	0.9636	1.1755	1.1043
1.5	1.800	1.3375	0.4910	1.4800	1.8003	1.1894
2	2.9471	2.1865	0.7389	2.3066	2.8184	1.7607

Table 4.3: Normalized l_2-norm values between the default trajectory of each variable and the trajectories obtained when changing parameter β_1. The l_2-norms were normalized with the default peak value of the respective variable.

Based on the l_2-norm values the parameter was classified as stable, partly stable and sensitive for each variable. Stable were those parameters that had an extremely small affect on the variables. Changing these parameters resulted in l_2-norm values in ranges of 1e-05 to 1e-01. Partly sensitive were parameters that resulted in l_2-norm values in the range of 1e-01 to 1 and sensitive were the parameters with l_2-norm values above 1. The parameters and their classifications for different variables can be seen in table 4.4.

Parameter	IFN	IL-8	Neutrophils	IL-6	IP-10	T-cells	Virus
β_1	Sensitive	Sensitive	PartlySensitive	Sensitive	Sensitive	Sensitive	Sensitive
β_2	Sensitive	Sensitive	Partly Sensitive	Sensitive	Sensitive	Sensitive	Sensitive
β_3	Sensitive	Sensitive	Partly Sensitive	Sensitive	Sensitive	Sensitive	Sensitive
β_4	Partly Sensitive	Partly Sensitive	Partly Sensitive	Partly Sensitive	Partly Sensitive	Partly Sensitive	Sensitive
β_5	Partly Sensitive	Partly Sensitive	Partly Sensitive	Partly Sensitive	Partly Sensitive	Sensitive	Sensitive
β_6	Partly Sensitive	Partly Sensitive	Partly Sensitive	Partly Sensitive	Partly Sensitive	Sensitive	Sensitive
β_7	Sensitive	Sensitive	Partly Sensitive	Sensitive	Sensitive	Sensitive	Sensitive
β_8	Stable	Sensitive	Partly Sensitive	Stable	Stable	Stable	Stable
β_9	Stable	Sensitive	Sensitive	Sensitive	Sensitive	Sensitive	Partly Sensitive
β_{10}	Stable	Stable	Sensitive	Stable	Stable	Stable	Stable
β_{11}	Stable	Stable	Sensitive	Stable	Stable	Stable	Stable
β_{12}	Stable	Stable	Stable	Stable	Stable	Stable	Stable
β_{13}	Stable	Stable	Stable	Stable	Stable	Stable	Stable
β_{14}	Stable	Stable	Stable	Sensitive	Stable	Stable	Stable
β_{15}	Stable	Stable	Stable	Stable	Sensitive	Sensitive	Partly Sensitive
β_{16}	Stable	Stable	Stable	Stable	Partly Sensitive	Partly Sensitive	Stable
β_{17}	Stable	Stable	Stable	Stable	Stable	Sensitive	Partly Sensitive
β_{18}	Stable	Stable	Stable	Stable	Stable	Partly Sensitive	Partly Sensitive
β_{19}	Stable	Stable	Stable	Stable	Stable	Stable	Stable
δ_v	Sensitive	Partly Sensitive	Partly Sensitive	Partly Sensitive	Sensitive	Sensitive	Sensitive
δ_T	Stable	Stable	Stable	Stable	Stable	Sensitive	Stable
g_S	Stable	Stable	Stable	Stable	Stable	Stable	Stable
g_C	Stable	Sensitive	Sensitive	Stable	Stable	Stable	Stable
g_N	Stable	Stable	Sensitive	Stable	Stable	Stable	Stable
g_L	Stable	Stable	Stable	Sensitive	Stable	Partly Sensitive	Stable

Table 4.4: Parameter - Variable sensitivity chart.

4.2.3 Use of the model to test two hypotheses

Elevated neutrophil levels

Mallia et al. showed in [1] that the number of neutrophils are higher in COPD patients than in controls during an infection. In order to test if these results also could be observed with the DDE model the parameters governing the baseline level of IL-8 (g_C), the baseline growth of neutrophils (g_N) and the neutrophil migration rate (β_{10}) were increased while changes of the neutrophil trajectory was observed. Before varying the parameters the initial condition was increased to the baseline level obtained in the COPD subjects.

Figure 4.3 shows the neutrophil trajectory when the parameters are changed one at a time. The result is presented with the COPD data in black and control data in blue. The red trajectory is the output of the DDE model.

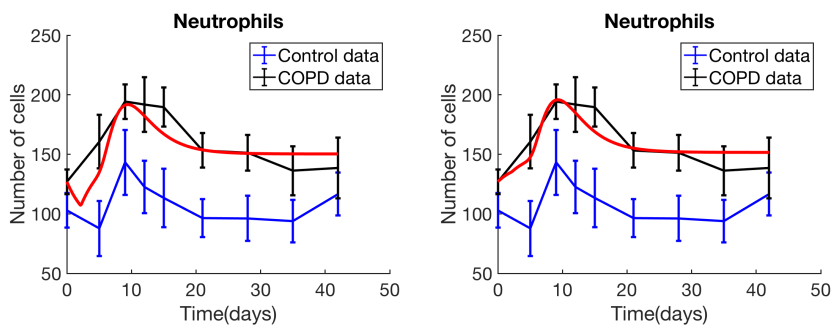

(a) Baseline growth of IL-8 increased with a factor 1.9

(b) Baseline growth of neutrophils increased with a factor 1.9

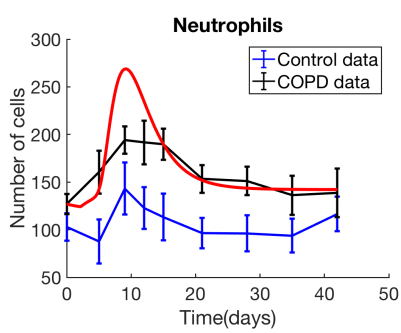

(c) Neutrophil migration rate increased with a factor 2.5

Figure 4.3: Result of increasing the parameters governing the baseline level of IL-8 (g_C), the baseline growth of neutrophils (g_N) and the neutrophil migration rate (β_{10}). Control data is presented in blue and COPD data is presented in black. The red trajectories represent the neutrophil quantity.

Impaired production of IFN-β

Based on the results in [1] Mallia et al. also suggested that a deficient IFN-β production may lead to increased susceptibility for COPD patients. The production rate of IFN-β by infected cells (β_5) and the production rate of IFN-β by dendritic cells (β_{13}) were decreased to 1e-05 of their respective default values and the changes in viral load was observed. When parameter β_5 was decreased the virus peak concentration increased to a peak of 5.4418 log_{10} copies/ml as seen in figure 4.4. When parameter β_{13} was decreased no considerable change of the virus trajectory could be observed.

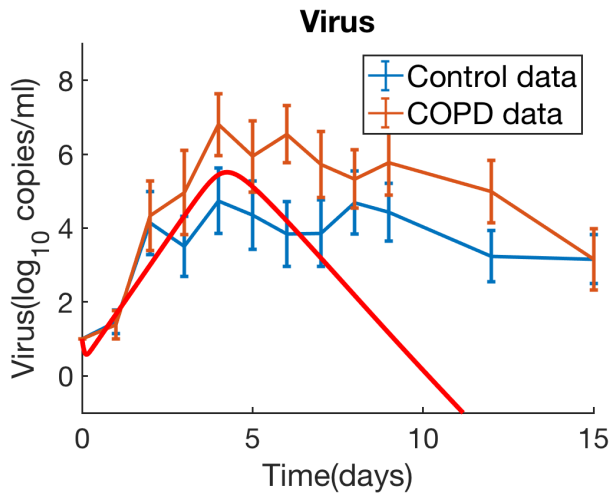

Figure 4.4: Result of decreasing the IFN-β production rate by infected cells (β_5) to 1e-05 of its default value. Data from COPD patients can be seen in orange with error bars, data from controls can be seen in blue with error bars and the red trajectory is the output from the DDE model.

4.3 Identifiability Analysis

In the first part of the identifiability analysis the data of virus from the upper respiratory tract was used for optimization. This resulted in 14 practically non-identifiable parameters and one structurally non-identifiable parameter which can be seen in table 4.5.

4.3.1 Resolving non-identifiabilities

After adding the data of IL-6 and IL-8 the identifiability analysis was performed anew. This yielded in 8 practically non-identifiable parameters and one structurally non-identifiable parameter of which can be seen in table 4.6.

Parameter	Non-identifiability
β_1	
β_2	
β_3	
β_4	
β_5	
β_6	
β_7	Practical
β_8	Practical
β_9	
β_{10}	Practical
β_{11}	Practical
β_{12}	Practical
β_{13}	Practical
β_{14}	Practical
β_{15}	Practical
β_{16}	Practical
β_{17}	Practical
β_{18}	
β_{19}	Practical
δ_V	
δ_T	Structural
g_S	Practical
g_C	Practical
g_N	Practical
g_L	

Table 4.5: Result of the identifiability analysis obtained when using the virus data for optimization. The parameters that are not marked with a non-identifiability were fully identifiable.

Parameter	Non-identifiability
β_1	
β_2	
β_3	
β_4	
β_5	
β_6	
β_7	
β_8	
β_9	
β_{10}	Practical
β_{11}	Practical
β_{12}	Practical
β_{13}	Practical
β_{14}	
β_{15}	Practical
β_{16}	Practical
β_{17}	
β_{18}	
β_{19}	Practical
δ_V	
δ_T	Structural
g_S	
g_C	
g_N	Practical
g_L	

Table 4.6: Result of the identifiability analysis performed using the data sets of virus, IL-8 and IL-6.

Chapter 5

Discussion

5.1 Model

The model was able to reproduce the data and the viral dynamics from the upper respiratory tract as well as IL-8 and neutrophil dynamics from the lower respiratory tract. For IFN-β, IP-10 and CD8+ T-cells there were no data available for fitting and reference values for some of the parameters could not be found in the literature. As a result this made it more difficult to determine the reliability of the the model dynamics of these variables. ODEs are valuable for studying viral dynamics in a well-mixed system, however the model presented in this thesis included both variables that are expressed locally at the site of infection, like cytokines, and variables that are not normally present in the tissue but migrate to the site of infection, like neutrophils. The spatial effects are likely important and a model that accounts for the location of different cells and molecules may better represent the dynamics.

Susceptible cells
The susceptible cells were modeled with a constant growth term, g_S. This was done in order to avoid the model becoming target limited since this is an unlikely situation *in vivo* where there will always be new epithelial cells for the virus to infect. According to Christopher McCrae, results from AstraZeneca have showed that infected cells returned to susceptible again during an HRV infection. This could be added to the model by a new state variable that accounts for the recovered cells. Another option could be to connect the infected and susceptible cells by adding two terms that account for the recovery. However this would result in more parameters to estimate.

Infected cells
The infected cells were initialized to zero and after the peak the quantity declined to 10 cells. For the parameters with reference boundaries from literature only the

killing rate of infected cells by CD8+ T-cells (β_{18}) got an estimate outside the reference range. However the reference, from [10], was an estimate made from killing rate by NK-cells and not a result of CD8+ T-cells from clinical experimentation.

Virus
The model was able to capture the dynamics of virus concentration. Between baseline and day 1 a rapid decrease appeared in the viral trajectory. This was because the model was initialized with 10 copies/ml of free virus and zero infected cells. Until a cell has been infected no viral production occurs and as a result the concentration decreased during the first day due to removal of free virions by mucus and normal decay. In the model the virus production was assumed to start as soon as target cells became infected but virus may also be released when infected cells lyse [10]. The proportion of virions released through cell lysis is not known which complicates the process of creating a model that accounts for both. Furthermore virus was modeled with a term representing the virions that infect the susceptible cells, $\beta_7 SV$. These virions were removed from the pool of free virus in the mucus and hence modeled as a decrease. Modeling the virus with a term like this has previously been done in [10] and [22].

IFN-β
From Mallia et al. there was no data available for IFN-β which made it difficult to validate the final result. IFN are known to be one of the first mediators of the innate immunological defence and they are usually present 1-2 days after the virus peak [3]. Based on these results the model seems to capture the peak time of IFN-β since it appears 4-5 dpi. which is approximately 1-2 days after the start of the virus peak. In this model IFN-β inhibit the viral replication through the term $\frac{\beta_3}{1+\beta_4 F}$ where β_3 is the virus production rate and β_4 is the effectiveness of IFN-β. This way of modeling the interference between IFN-β and virus has previously been used in [26]. For simplicity the DCs were modeled as a constant instead of a variable in this model.

IL-8
The model is able to capture the dynamics of IL-8 from the lower respiratory tract. The decay rate, β_9, was chosen to be the same for all cytokines in the model (IL-8, IL-6, IP-10 and IFN) in order to keep the number of parameters as low as possible. The parameter range that was used as reference for fitting was large and the final estimate seemed to give a good fit for IL-8.

Neutrophils
The model was able to capture the neutrophil data from the lower respiratory tract well. In the data from the lower respiratory tract the baseline level was non zero

and the quantity decreases to the same levels after the peak has occurred. These results suggest that a baseline migration that is not dependent on the infection is needed in order to replicate the clinical results. The delay used on the migration rate of neutrophils from IL-8 was necessary to get the peak to accord with data.

IL-6

The results show that the model was not sufficient to describe the dynamics of IL-6 from the lower respiratory tract. After discussion with Hoda Sharifian at AstraZeneca the conclusion was made that one reason for this may be that macrophages, which function as important producers of IL-6, were excluded from the model. The delay of 80 hours, added to the production of IL-6 by infected cells, was necessary to get the peak at 9-10 dpi. By adding the macrophages as a variable the delay could possibly have been removed resulting in a slower increase of IL-6.

IP-10

For IP-10 there were no data available from the study by Mallia et al. In [22] Mitchel et al. report that human bronchial epithelial cells, after being infected with three types of influenza virus strains in vitro, expressed IP-10 already after 8 hours post infection and according to their data peaked 2-3 dpi. The model developed in this thesis indicated that IP-10 increase started 3 dpi. and peaked 6 dpi. which is clearly delayed compared to the data presented by Mitchel et al. Indeed a delay of 30 hours was added to the IP-10 equation but this was necessary in order to delay the response of CD8+ T-cells. However, the peak concentration and time may be larger and earlier in vitro than in vivo since in vitro experiments do not include other biological mechanisms that is part of the immune response in the human body. Furthermore Mitchel et al. only collected data for the first 72 hours.

CD8+ T-cells

For CD8+ T-cells there were no data available from the study by Mallia et al. The T-cells are part of the adaptive immune response and arrive to the cite of infection after they have been activated by dendritic cells. Hence they are not observed until 1-2 weeks after the infection starts [14]. The CD8+ T-cell trajectory showed a peak at 9-11 dpi which could be a valid estimation according to literature. The migration of CD8+ T-cells was induced by IL-6 and IP-10 in the model but reference boundaries of which of them that accounts for the major production could not be found.

5.2 Sensitivity Analysis

A sensitivity analysis was performed on 25 of the parameters in the DDE model. The parameters that were excluded were the time constants τ_1, τ_2, τ_3 in the delay equations. These delays were part of the equations governing the peaks of IL-6, neutrophils and IL-8. Small changes of the peak time for these variables appeared to only notably effect the dynamics of the other variables and therefore they were excluded from the sensitivity analysis.

5.2.1 Virus sensitivity

Results from the first part of the sensitivity analysis, when only the sensitivity of virus was observed as the parameters were varied, showed that the virus was sensitive for parameter β_1 to β_7 as well as δ_V. This was expected since these parameters are connected to either the production or decrease of infected cells, IFN-β or the virus itself. Based on the trajectories plotted as each of the parameters were varied, shown in figure A.1, the virus was most sensitive in the end of the infection period. Parameter β_1 to β_7 and δ_V seemed to have the biggest effect on the virus. The peak seemed to be mostly sensitive for changes of β_2, β_7 and δ_V whereas the time of the peak was most sensitive for changes of β_1, β_3 and β_7. To achieve more accurate results a more detailed sensitivity analysis with individual boundaries for each parameters should preferably be performed. For some parameters a variation from 0.5 to 2 times the initial estimate is not enough to be able to make conclusions whether it has an impact on viral load or not. Larger variations were tested throughout the analysis but for some parameters the system became unstable and since it was desirable to use the same ranges for all parameters in order to maintain the structure through the analysis the the safer ranges between 0.5 an 2 were used.

5.2.2 Sensitivity of the other variables

In the second part of the analysis the sensitivity of all variables except infected and susceptible cells were observed as the parameters were varied. The result was used to construct a parameter - variable sensitivity chart. In this table it is possible to read that all the variables, except neutrophils, are sensitive for changes in the infection rate (β_1) and turn over rate of infected cells (β_2) since the production of these variables is directly dependent on the number of infected cells. Neutrophils are not directly connected to infected cells but depend on the production of IL-8 which makes the variable partly sensitive for β_1 and β_2. Moreover all variables

are either partly sensitive or sensitive to the production and decay rates of virus and IFN-β, parameter β_3 to β_7 and δ_V.

Surprisingly the virus is stable for changing the killing rate of infected cells by neutrophils (β_{12}) and partly sensitive for changes of the killing rate by CD8+ T-cells (β_{18}). This suggests that most of the infection is cleared by T-cells rather than neutrophils. Furthermore the CD8+ T-cells are more sensitive to changes of the migration rate by IP-10 than of IL-6. This implies that it might be more important to compliment this study with data for IP-10, if available, rather than to search for data for IL-6 from the upper respiratory tract.

5.2.3 Use of the model to test two hypotheses

Elevated neutrophil levels
In this hypothesis the three parameters baseline growth of neutrophils (g_N), baseline growth of IL-8 (g_C) and neutrophil migration rate (β_{10}) were increased while changes in the neutrophil trajectory were observed. Compared to changes of the neutrophil migration rate(figure 4.3b), increasing the baseline growth of IL-8 (figure 4.3a) and the neutrophilic growth rate (figure 4.3c) resulted in neutrophil dynamics that more closely captured COPD data. These results suggest that increased neutrophil levels in COPD patients is due to increased baseline levels rather than an increased migration rate.

Deficient production of IFN-β
When this hypothesis was tested the parameters governing IFN-β production by infected cells (β_5) and dendritic cells (β_{13}) were decreased and changes of the viral load was observed. As can be seen in figure 4.4, an impaired IFN-β production by infected cells does not result in increased virus levels comparable to COPD. However there are controversial results regarding the deficiency of IFN-β production since experiments have been performed on different cell types and different cell types express IFN-β differently.

As the parameter governing the production by dendritic cells was varied no changes were observed in viral concentration. Results from the sensitivity analysis, presented in the sensitivity chart 4.4, also indicated that virus was not effected at all by changes of β_{13} but the results indicating on the stability of this parameter were more prominent here as it was decreased to 1e-05 of its original value. According to these results the production by dendritic cells is negligible which is unlikely since it is known that dendritic cells act as an important producer of IFN-β, according to Christopher McCrae at AstraZeneca. Therefore a suggestion is to add

the dendritic cells as a variable to be able to study its dynamics.

5.3 Identifiability Analysis

The identifiability analysis gave 14 practically non-identifiable parameters. These parameters were all either classified as stable or partly sensitive in the sensitivity analysis on virus except for the infection rate of susceptible cells (β_7) that was classified as sensitive. For these practically non-identifiable parameters the data contains information about the parameter but not enough to make them identifiable. CD8+ T-cell decay rate was the only parameter obtained structurally non-identifiable. This parameter was classified as stable in the sensitivity analysis and together with the results from the identifiability analysis this implies that the model is not sufficient to describe its dynamics.

5.3.1 Resolving non-identifiabilities

After the data sets of IL-8 and IL-6 was added, 6 of the practically non-identifiable parameters could be resolved. The ones that remained non-identifiable were parameters connected to variables for which there were no data utilized, as for example β_{15} governing the production of IP-10 and β_{16} governing production of CD8+ T-cells.

Parameter δ_T remained structurally non-identifiable since it is not possible to resolve a structurally non-identifiable parameter by adding more data. Since this parameter was also marked as stable in the sensitivity analysis it could probably be removed from the equation without effecting the overall dynamics of either virus nor CD8+ T-cells.

5.4 Future Perspective

The next step in this project would have been to use the results from the identifiability analysis to reduce the model by removing reactions that would not effect the viral dynamics and that cannot be uniquely estimated with the available data. Furthermore dendritic cells and macrophages would have been added as variables to the model in order to better be able to describe IL-6 dynamics and the dynamics of IFN-β governed by dendritic cells. It would also be of interest to fit the DDE model to COPD data and observe how and which parameters that changed.

A second step would be to redo the sensitivity analysis with individual ranges for each parameter. By exploring the extremes of each parameter it would be possible to make more accurate conclusions about their respective sensitivity. If so

then the results presented in the sensitivity chart could possibly be used directly to give answer to hypotheses made about the dynamics.

The long term goal would be to connect the DDE model with a spatial model. Such a spatial model has in parallel with this project been developed by another master thesis student at the Center of Systems Biology in Dresden. If this could be done successfully then the spatiotemporal model could be used to run simulations of how the infection front propagates from the upper to the lower respiratory tract while being battled by the immune system. With such a model it could be possible to investigate if the concentrations of inflammatory cells and cytokines differ between the upper and lower respiratory tracts and between controls and COPD patients. It could also be possible to investigate the importance of mucus movement for accumulation of inflammatory cells and cytokines and the effects this would have on the viral spread.

5.5 Ethical reflection

The data that was utilized in this thesis came from an experiment during which COPD patients were infected with HRV. After inoculation the symptoms of the subjects worsened to such a degree that all patients fulfilled the criteria for a COPD exacerbation. Because the exacerbations were triggered as a result of the infection, samples could be collected both before, during and after the exacerbation period. The results from this type of controlled study were valuable in the sense of studying the pathogenesis of HRV compared to studies performed on patients having naturally occuring exacerbations.

However, since the exacerbations can be life-threatening for the patients ethical approval from both authorities and the participants were required. The health risks were high and since the patients could only be given symptom relieving medication these types of studies are controversial.

One of the difficulties with developing all kind of pharmaca is that tests eventually have to be performed on humans. To a certain extent the computational, *in situ*, models can be used as a complement or alternative to the experimental models. If the model developed in this thesis successfully could be integrated in a spatial model the dynamics of virus and inflammatory cells could be simulated and tests that would otherwise have been performed during clinical experimentation could instead be tested on the model.

Chapter 6

Conclusion

In this thesis a temporal model of the immune system during a virus infection was developed. It includes immunological mechanisms that are believed to occur during a COPD exacerbation triggered by a respiratory infection of Human Rhinovirus. The model was used to derive numerical values of kinetics in the immune response and of the infection dynamics. By a sensitivity analysis it was outlined which parameters of the model that may be of importance for the immune system to clear the viral infection. An identifiability analysis showed that the model and the available data were sufficient to describe the dynamics. If connected to a spatial model, the model can in the future be used to simulate the viral and immune dynamics in the human lung.

Chapter 7

Variable & parameter definitions

Symbol	Definition
S	Susceptible epithelial cells
I	Infected epithelial cells
V	Free virions
F	Free IFN-β
C	Free IL-8
N	Neutrophils
L	Free IL-6
P	Free IP-10
T	CD8+ T-cells
DC	Dendritic cells in the epithelial tissue

Table 7.1: Variable definitions.

Parameter	Definition
β_1	Infection rate of susceptible cells
β_2	Decay rate of infected cells
β_3	Virus production rate
β_4	Inhibition of viral production by IFN
β_5	Production of IFN by infected cells
β_6	Decay rate of IFN
β_7	Infection rate of susceptible cells
β_8	Production rate of IL-8
β_9	Decay rate of IL-8
β_{10}	Migration rate of neutrophils
β_{11}	Decay rate of neutrophils
β_{12}	Kill rate by neutrophils
β_{13}	Production rate of IFN by DC
β_{14}	Production rate of IL-6
β_{15}	Production rate of IP-10
β_{16}	Migration rate of T-cells by IL-6
β_{17}	Migration rate of T-cells by IP-10
β_{18}	Kill rate by T-cells
β_{19}	Apoptosis rate induced by IFN
δ_V	Virus decay rate
δ_T	T-cell decay rate
g_S	Baseline growth of susceptible cells
g_C	Baseline growth of IL-8
g_N	Baseline growth of neutrophils
g_L	Baseline growth of IL-6

Table 7.2: Parameter definitions.

Bibliography

[1] V. Gielen M. Contoli K. Gray T. Kebadze J. Aniscenko V. Laza-Stanca M.R Edwards L. Slater A. Papi L.A Stanciu O.M Kon M. Johnson S.L Johnston P. Mallia, S.D Message. Experimental Rhinovirus Infection as a Human Model of Chronic Obstructive Pulmonary Disease Exacerbation. *Am J Respir Crit Care Med.*, 183(6):734–42, 2011.

[2] K. St. George T.J. Walsh S.E. Jacobs, D.M. Lamson. Human Rhinoviruses. *Clin Microbiol Rev.*, 26(1):135–162, 2013.

[3] J. Stock S. Kirchberger, O. Majdic. Modulation of the immune system by human rhinoviruses. *International Archives of Allergy and Immunology*, 142(1):1–10, 2007.

[4] S. Avdeev G. Di Maria C.F.Donner J. Luis Izquierdo N. Roche T. Similowski-H. Watz H.Worth A. Rossi, Z.Aisanov and M. Miravitlles. Mechanisms, assessment and therapeutic implications of lung hyperinflation in COPD. *Respiratory Medicine*, 109:785–802, 2015.

[5] W. MacNee. Pathogenesis of Chronic Obstructive Pulmonary Disease. *American Thoracic Society*, page 258–266, 2005.

[6] G.J. Criner V. Kim. Chronic Bronchitis and Chronic Obstructive Pulmonary Disease.. *American Thoracic Society*, 187(3):228–237, 2013.

[7] S. Mizuno NF. Voelkel, J. Gomez-Arroyo. COPD/emphysema: The vascular story. *Pulmonary Circulation*, 1(3):320–326, 2011.

[8] Harvard. Emphysema.

[9] P.M. Howley B.N. Fields, D.M. Knipe. *Fields Virology, 3rd ed.* Lippincott-Raven Publishers, Philadelphia, USA, 1996.

[10] P.S. Kim F.R. Adler. Models of contrasting strategies of rhinovirus immune manipulation. *Journal of Theoretical Biology*, 327:1–10, 2013.

[11] A. Järvinen T. Heikkinen. The common cold. *The Lancet*, 361(9351):51–9, 2013.

[12] SL. Johnston A. Papi. Rhinovirus infection induces expression of its own receptor intercellular adhesion molecule 1 (ICAM-1) via in- creased NF-kB-mediated transcript. *The Journal of Biological Chemistry*, 274(14):9707–20, 1999.

[13] https://www.quora.com/Are-NK-T-cells-part-of-the-innate-or-the-specific-immune system. Immune cells.

[14] S. Pillai A.K. Abbas, A.H. Lichtman. *Cellular and Molecular Immunology, 7th edition*. Elsevier Saunders, Philadelphia, USA, 2012.

[15] S. Weston-R. Latham-H.K Muller-S.S Sohal-E.H Walters S.D Shukla, M.Q Mahmood. The main rhinovirus respiratory tract adhesion site (ICAM-1) is upregulated in smokers and patients with chronic airflow limitation (CAL).. *Respiratory Research*, 18:6, 2017.

[16] A.T Comstock-C.A Meldrum-R. Mahidhara-A.M Goldsmith-J.L Curtis F.J Martinez-M.B Hershenson U. Sajjan D. Schneider, S. Ganesan. Increased Cytokine Response of Rhinovirus- infected Airway Epithelial Cells in Chronic Obstructive Pulmonary Disease.. *American Journal of Respiratory and Critical Care Medicine*, 182(3):332–40, 2010.

[17] R.J Sapsford-J.A Wedzicha A. Bhowmik, T.A Seemungal. Relation of sputum inflammatory markers to symptoms and lung function changes in COPD exacerbations. *HTORAX*, 55(2):114–20, 2000.

[18] M. Contoli-K. Gray-A. Telcian-V. Laza-Stanca A. Papi L.A Stanciu S. Elkin O.M Kon M. Johnson S.L Johnston P. Mallia, S.D Message. Lymphocyte subsets in experimental rhinovirus infection in chronic obstructive pulmonary disease. *Respiratory Medicine*, 108(1):78–85, 2014.

[19] R. Albert-G.H. Long-R. Zhang J. Thakar, M. Poss. Dynamic models of immune responses: what is the ideal level of detail?. *Theoretical Biology and Medical Modelling*, 7(35), 2010.

[20] S. Motta F. Pappalardo. Mathematical modeling of biological systems. *Briefings in Bioinformatics*, 14(4):411–22, 2013.

[21] D. Kaschek-J. Timmer C. Kreutz, A. Raue. Profile likelihood in systems biology. *FEBS Journal*, 280(11):2564–71, 2013.

[22] S.Forrest C.A.A. Beauchemin-J. Tipper-J. Knight-N. Donart-R.C. Layton J. Pyles P. Gao K.S. Harrod A.S. Perelson F. Koster H.Mitchell, D. Levin.

Higher Level of Replication Efficiency of 2009 (H1N1) Pandemic Influenza Virus than Those of Seasonal and Avian Strains: Kinetics from Epithelial Cell Culture and Computational Modeling. *Journal of Virology*, 85(2):1125–1135, 2011.

[23] S. Banerjee-C.Clay J. Cannon M. Moses F.Koster D. Levin, S. Forrest. A spatial model of the efficiency of T cell search in the influenza-infected lung. *Journal of Theoretical Biology*, 398:52–63, 2016.

[24] G.A. Bocharov G.I. Marchuk, A.A. Romanyukhat. Mathematical Model of Antiviral Immune Response. II. Parameters Identification for Acute Viral Hepatitis B. *Journal of Theoretical Biology*, 151:41–70, 1991.

[25] C. Kreutz C. Tonsing, J. Timmer. Profile likelihood based analyses of infectious disease models. *SAGE Journals*, 27(7):1979–98, 2018.

[26] C.A Macken-F.G Hayden A.S. Perelson P. Baccam, C. Beauchemin. Kinetics of Influenza A Virus Infection in Humans. *Journal of Virology*, 80(15):7590–6, 2006.

[27] J. Sarkar-B. Kubiak C. Ziraldo J. Dutta-Moscato et al. G. Nieman, D. Brown. A Two-Compartment Mathematical Model of Endotoxin-induced Inflammatory and Physiologic Alterations in Swine. *Critical care Medicine*, 40(4):1052–1063, 2012.

[28] D. Swigon B.G. Ermentrout S. Lukens F.R. Toapanta T.M. Ross G. Clermont I. Price, E.D. Mochan-Keef. The inflammatory response to influenza A virus (H1N1): an experimental and mathematical study. *Journal of Theoretical Biology*, 7(374):83–93, 2015.

[29] A.A Pinto M. Ferreira N.J. Burroughs, B.M.P.M. Oliveir. Immune response dynamics. *Mathematical and Computer Modelling*, 53(7-8):1410–19, 2011.

[30] T. Suzuki N. Yamada M. Furukawa S. Ishizuka K. Nakayama M. Terajima Y. Numazaki H. Sasaki M. Yamaya, K. Sekizawa. Infection of human respiratory submucosal glands with rhinovirus: effects on cytokine and ICAM-1 production. *American Journal of Physiology*, 277(2 Pt 1):362–71, 1999.

[31] T. Maiwald J. Bachmann M. Schilling U. Klingmüller J. Timmer A. Raue, C. Kreutz. Structural and practical identifiability analysis of partially observed dynamical models by exploiting the profile likelihood. *Bioinformatics*, 25(15):1923–1929, 2009.

[32] S. H. Moolgavkar D.J. Venzon. A Method for Computing Profile-Likelihood-Based Confidence Intervals. *Applied Statistics*, 37(1):87–94, 1988.

[33] U. Klingmüller J. Timmer A. Raue, V. Becker. Identifiability and observability analysis for experimental design in nonlinear dynamical models. *Chaos: An Interdisciplinary Journal of Nonlinear Science*, 20(4), 2010.

Appendices

Appendix A

Graphical results from sensitivity analysis performed on virus

Here the trajectories from the sensitivity analysis performed on virus is shown. The parameters that are presented are β_1 to g_L. In the figures the virus trajectory obtained with the default parameter value can be seen in dark blue whilst the trajectories obtained with the modified parameters have lighter colours.

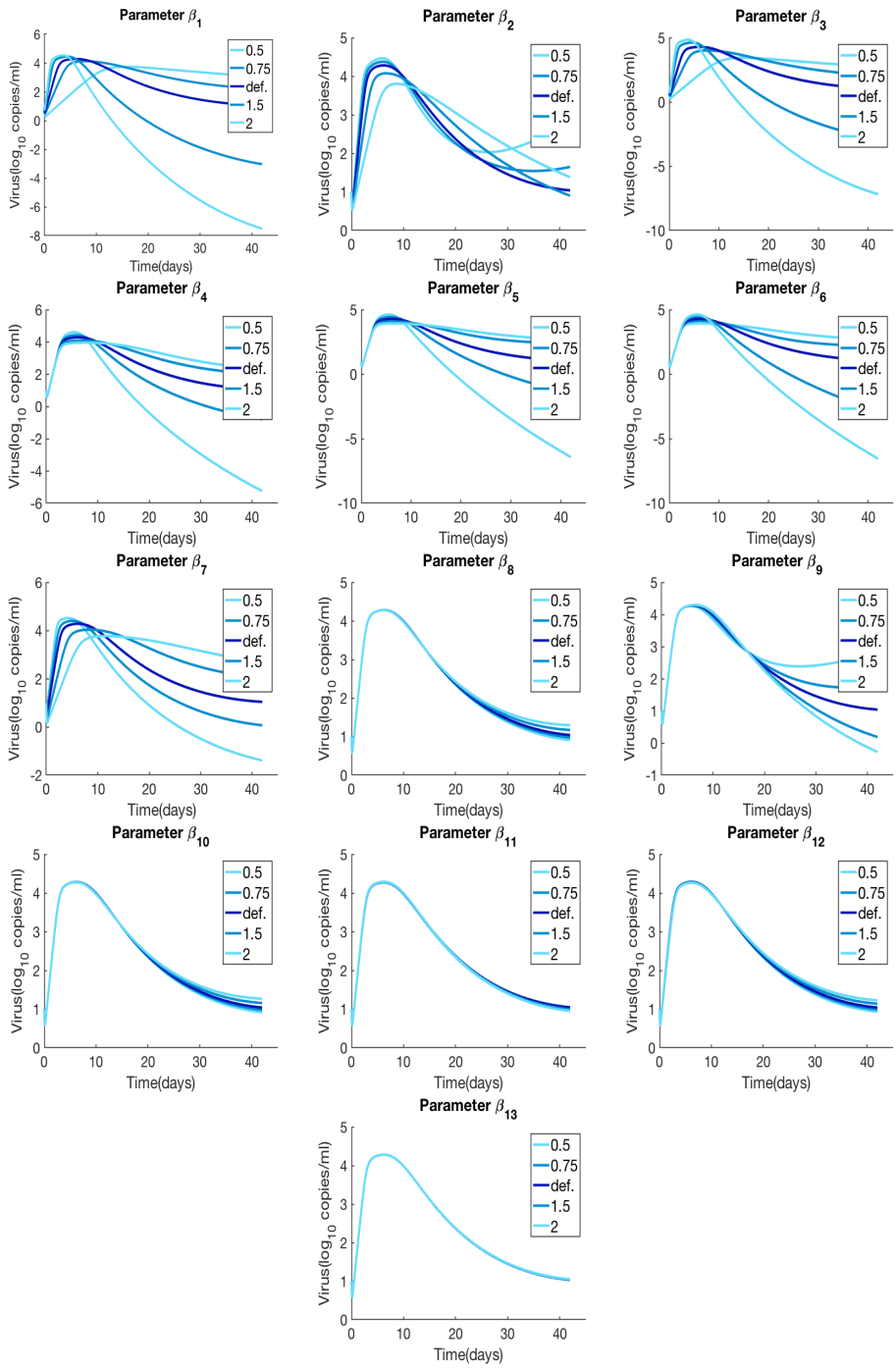
Parameter β_1
Parameter β_2
Parameter β_3
Parameter β_4
Parameter β_5
Parameter β_6
Parameter β_7
Parameter β_8
Parameter β_9
Parameter β_{10}
Parameter β_{11}
Parameter β_{12}
Parameter β_{13}
Virus($\log_{10}$ copies/ml)
Time(days)
0.5
0.75
def.
1.5
2

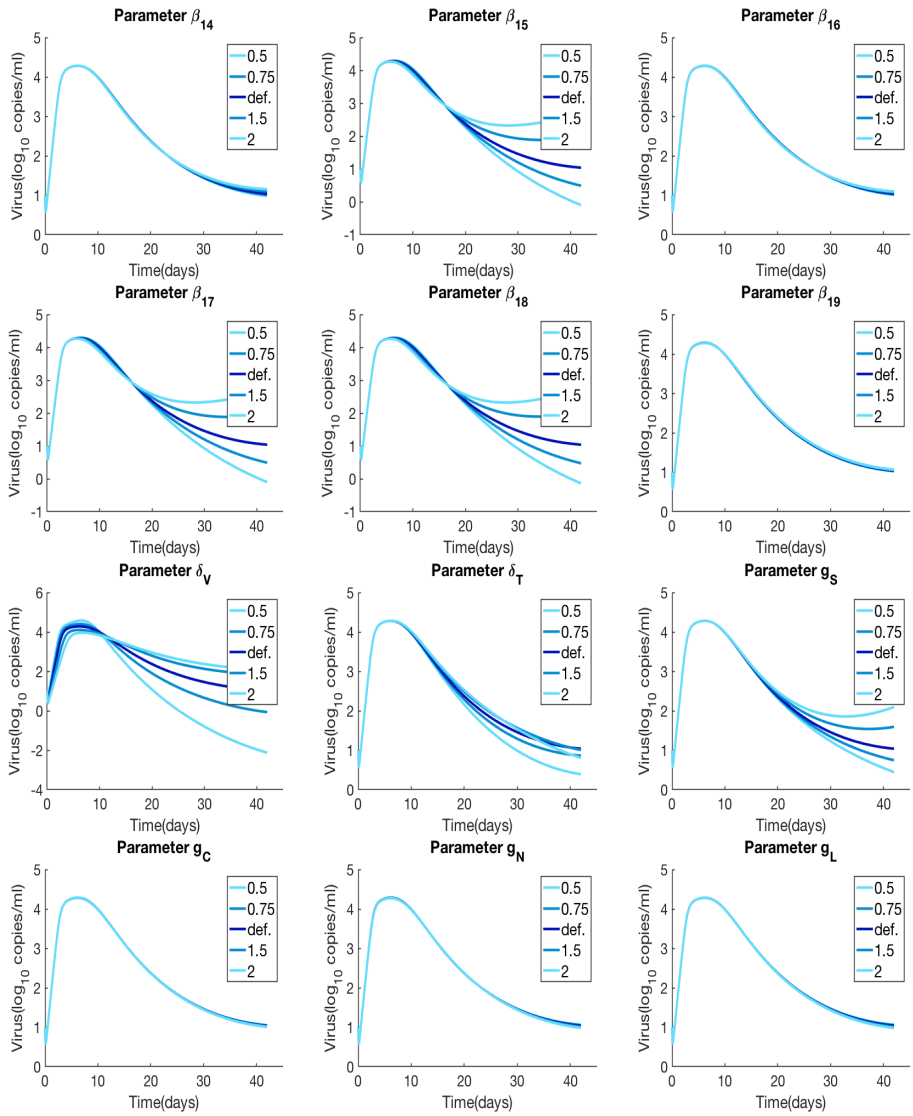

Figure A.1: Virus load during sensitivity analysis.

Appendix B

Complete collection of l_2-norms from extended sensitivity analysis

Here the normalized l_2-norms from the extended sensitivity analysis is presented. Each table belongs to a specific parameter. On the left the parameter variations 0.5 to 2 is shown and in the following columns the normalized l_2-norm outputs from the variations for each variable can be seen.

Parameter β_1. L2 norms						
Parameter change	IFN	IL-8	Neutrophils	IL-6	IP-10	T-cells
0.5	1.8857	1.4017	0.7988	1.5220	1.8578	2.6650
0.75	1.1918	0.8859	0.4003	0.9636	1.1755	1.1043
1.5	1.800	1.3375	0.4910	1.4800	1.8003	1.1894
2	2.9471	2.1865	0.7389	2.3066	2.8184	1.7607

Parameter β_2. L2 norms						
Parameter change	IFN	IL-8	Neutrophils	IL-6	IP-10	T-cells
0.5	1.8889	1.4041	0.7095	1.5147	1.8497	2.4686
0.75	0.7596	0.5642	0.2861	0.6076	0.7416	0.9931
1.5	0.9898	0.7358	0.3766	0.8015	0.9774	1.2934
2	1.5947	1.1854	0.6314	1.2880	1.5715	2.1845

Parameter β_3. L2 norms						
Parameter change	IFN	IL-8	Neutrophils	IL-6	IP-10	T-cells
0.5	1.8663	1.3874	0.7821	1.5066	1.8388	2.5887
0.75	1.1359	0.8443	0.3825	0.9186	1.1203	1.0587
1.5	1.7382	1.2926	0.4746	1.4365	1.7492	1.1521
2	2.8737	2.1277	0.7197	2.2386	2.7335	1.7161

Parameter β_4. L2 norms						
Parameter change	IFN	IL-8	Neutrophils	IL-6	IP-10	T-cells
0.5	0.9211	0.6839	0.2532	0.7398	0.9037	0.6207
0.75	0.3762	0.2795	0.1130	0.3033	0.3704	0.2846
1.5	0.4795	0.3564	0.1673	0.3868	0.4722	0.4602
2	0.7667	0.5698	0.2817	0.6188	0.7552	0.8089

Parameter β_5. L2 norms						
Parameter change	IFN	IL-8	Neutrophils	IL-6	IP-10	T-cells
0.5	0.7162	0.7017	0.2691	0.7590	0.7042	1.2168
0.75	0.3256	0.2847	0.1190	0.3088	0.3200	0.5833
1.5	0.5219	0.3589	0.1734	0.3897	0.5134	1.0787
2	0.9317	0.5719	0.2900	0.6211	0.9165	2.0438

Parameter β_6. L2 norms						
Parameter change	IFN	IL-8	Neutrophils	IL-6	IP-10	T-cells
0.5	0.9288	0.5610	0.2850	0.6087	0.9141	2.0467
0.75	0.3621	0.2557	0.1212	0.2774	0.3562	0.7324
1.5	0.4477	0.3963	0.1624	0.4297	0.4403	0.7886
2	0.7179	0.6864	0.2648	0.7426	0.7062	1.2194

Parameter β_7. L2 norms						
Parameter change	IFN	IL-8	Neutrophils	IL-6	IP-10	T-cells
0.5	1.5168	1.1290	0.4053	1.2443	1.5172	0.9726
0.75	0.7454	0.5532	0.2058	0.5853	0.7157	0.5050
1.5	1.1437	0.8500	0.3852	0.9248	1.1278	1.0492
2	1.7538	1.3037	0.6719	1.4164	1.7281	2.0138

Parameter β_8. L2 norms						
Parameter change	IFN	IL-8	Neutrophils	IL-6	IP-10	T-cells
0.5	0.00093	0.6761	0.3972	0.0075	0.0092	0.0141
0.75	0.0047	0.3376	0.1982	0.0038	0.0046	0.0070
1.5	0.0091	0.6726	0.3942	0.0074	0.0090	0.0139
2	0.0182	1.3418	0.7854	0.0148	0.0180	0.0275

Parameter β_9. L2 norms						
Parameter change	IFN	IL-8	Neutrophils	IL-6	IP-10	T-cells
0.5	0.1835	2.3849	1.6093	2.0473	1.5665	2.6867
0.75	0.0676	0.8052	0.5451	0.6961	0.5419	0.9425
1.5	0.0766	0.8221	0.5576	0.7158	0.5661	1.0040
2	0.1188	1.2407	0.8421	1.0824	0.8605	1.5332

Parameter β_{10}. L2 norms						
Parameter change	IFN	IL-8	Neutrophils	IL-6	IP-10	T-cells
0.5	0.0163	0.0121	0.8719	0.0131	0.0160	0.0285
0.75	0.0081	0.0060	0.4352	0.0065	0.0080	0.0142
1.5	0.0159	0.0118	0.8662	0.0128	0.0156	0.0279
2	0.0315	0.0235	1.7270	0.0255	0.0311	0.0553

Parameter β_{11}. L2 norms						
Parameter change	IFN	IL-8	Neutrophils	IL-6	IP-10	T-cells
0.5	0.0506	0.0376	4.2193	0.0409	0.0498	0.0864
0.75	0.0216	0.0160	1.4739	0.0174	0.0213	0.0358
1.5	0.0292	0.0217	1.5391	0.0236	0.0288	0.0459
2	0.0473	0.0352	2.3322	0.0383	0.0466	0.0731

Parameter β_{12}. L2 norms						
Parameter change	IFN	IL-8	Neutrophils	IL-6	IP-10	T-cells
0.5	0.0559	0.0415	0.0226	0.0450	0.0549	0.0818
0.75	0.0277	0.0206	0.0112	0.0224	0.0272	0.0405
1.5	0.0543	0.0404	0.0218	0.0437	0.0527	0.0788
2	0.1070	0.0795	0.0429	0.0862	0.1048	0.1548

Parameter β_{13}. L2 norms						
Parameter change	IFN	IL-8	Neutrophils	IL-6	IP-10	T-cells
0.5	7.9e-04	3.9e-04	1.9e-04	4.3e-04	7.7e-04	0.0015
0.75	3.9e-04	1.7e-04	9.6e-05	2.1e-04	3.9e-04	7.4e-04
1.5	7.8e-04	3.9e-04	1.9e-04	4.2e-04	7.7e-04	0.0015
2	0.0016	7.8e-04	3.8e-04	8.5e-04	0.0015	0.0029

Parameter β_{14}. L2 norms						
Parameter change	IFN	IL-8	Neutrophils	IL-6	IP-10	T-cells
0.5	0.0038	0.0027	0.0016	0.7359	0.0036	0.1007
0.75	0.0020	0.0014	8.2e-04	0.3678	0.0019	0.0503
1.5	0.0034	0.0026	0.0016	0.7351	0.0035	0.1004
2	0.0071	0.0053	0.0032	1.4702	0.0069	0.2005

Parameter β_{15}. L2 norms						
Parameter change	IFN	IL-8	Neutrophils	IL-6	IP-10	T-cells
0.5	0.0962	0.0715	0.0419	0.0776	0.8702	1.3563
0.75	0.0464	0.0345	0.0202	0.0375	0.4288	0.6632
1.5	0.0843	0.0627	0.0365	0.0680	0.8247	1.2487
2	0.1599	0.1189	0.0690	0.1288	1.6124	2.4112

Parameter β_{16}. L2 norms						
Parameter change	IFN	IL-8	Neutrophils	IL-6	IP-10	T-cells
0.5	0.0065	0.0048	0.0032	0.0053	0.0064	0.2074
0.75	0.0033	0.0024	0.0016	0.0026	0.0032	0.1036
1.5	0.0065	0.0048	0.0032	0.0052	0.0064	0.2067
2	0.0129	0.0096	0.0063	0.0104	0.0127	0.4127

Parameter β_{17}. L2 norms						
Parameter change	IFN	IL-8	Neutrophils	IL-6	IP-10	T-cells
0.5	0.0962	0.0715	0.0419	0.0776	0.0947	1.3563
0.75	0.0464	0.0345	0.0202	0.0375	0.0457	0.6632
1.5	0.0843	0.0627	0.0265	0.0680	0.0830	1.2487
2	0.1599	0.1189	0.0690	0.1288	0.1574	2.4112

Parameter β_{18}. L2 norms						
Parameter change	IFN	IL-8	Neutrophils	IL-6	IP-10	T-cells
0.5	0.1027	0.0763	0.0455	0.0829	0.1012	0.1725
0.75	0.0494	0.0367	0.0218	0.0399	0.0487	0.0827
1.5	0.0891	0.0662	0.0392	0.0718	0.0878	0.1477
2	0.1683	0.1251	0.0738	0.1355	0.1656	0.2762

Parameter β_{19}. L2 norms						
Parameter change	IFN	IL-8	Neutrophils	IL-6	IP-10	T-cells
0.5	0.0137	0.0102	0.0048	0.0111	0.0135	0.0152
0.75	0.0068	0.0051	0.0024	0.0055	0.0067	0.0075
1.5	0.0134	0.0100	0.0047	0.0108	0.0132	0.0148
2	0.0265	0.0197	0.0093	0.0213	0.0260	0.0293

Parameter δ_V. L2 norms						
Parameter change	IFN	IL-8	Neutrophils	IL-6	IP-10	T-cells
0.5	0.7567	0.5617	0.2334	0.5972	0.7295	0.6295
0.75	0.3477	0.2578	0.1102	0.2748	0.3355	0.3035
1.5	0.5675	0.4217	0.1899	0.4626	0.5635	0.5465
2	1.0174	0.7562	0.3490	0.8232	1.0039	1.0278

Parameter δ_T. L2 norms						
Parameter change	IFN	IL-8	Neutrophils	IL-6	IP-10	T-cells
0.5	0.0212	0.0157	0.0105	0.0171	0.0208	1.9042
0.75	0.0102	0.0076	0.0051	0.0082	0.0101	0.7501
1.5	0.0184	0.0137	0.0090	0.0149	0.0182	0.8998
2	0.0344	0.0255	0.0168	0.0278	0.0339	1.4161

Parameter $_S$. L2 norms						
Parameter change	IFN	IL-8	Neutrophils	IL-6	IP-10	T-cells
0.5	0.0053	0.0039	0.0028	0.0043	0.0052	0.0124
0.75	0.0027	0.0020	0.0014	0.0021	0.0026	0.0063
1.5	0.0055	0.0041	0.0028	0.0044	0.0054	0.0129
2	0.0114	0.0085	0.0058	0.0090	0.0111	0.0267

Parameter $_C$. L2 norms						
Parameter change	IFN	IL-8	Neutrophils	IL-6	IP-10	T-cells
0.5	0.0079	0.8240	0.5791	0.0063	0.0077	0.0127
0.75	0.0039	0.4120	0.2896	0.0032	0.0039	0.0063
1.5	0.0078	0.8240	0.5791	0.0063	0.0077	0.0126
2	0.0156	1.6481	1.1582	0.0126	0.0153	0.0252

Parameter $_N$. L2 norms						
Parameter change	IFN	IL-8	Neutrophils	IL-6	IP-10	T-cells
0.5	0.0252	0.0188	1.4226	0.0204	0.0249	0.0383
0.75	0.0126	0.0094	0.7113	0.0102	0.0124	0.0191
1.5	0.0249	0.0185	1.4226	0.0201	0.0245	0.0378
2	0.0494	0.0367	2.8453	0.0399	0.0487	0.0751

Parameter $_L$. L2 norms						
Parameter change	IFN	IL-8	Neutrophils	IL-6	IP-10	T-cells
0.5	0.0045	0.0033	0.0020	0.5824	0.0045	0.1238
0.75	0.0022	0.0017	9.8e-04	0.2913	0.0022	0.0619
1.5	0.0045	0.0033	0.0019	0.5826	0.0043	0.1238
2	0.0089	0.0066	0.0039	1.1651	0.0086	0.2477

Appendix C

Likelihood Profiles from identifiability analysis

Here the profile likelihoods for the identifiability analysis is presented. The analysis was performed on parameter β_1 to g_L. In the figures the asterisks mark the parameter value that yielded the best fit and the red dashed line demonstrates the 95% confidence level.

Parameter β_1

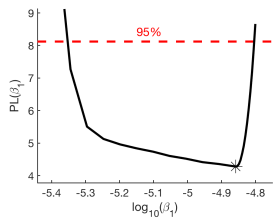

Parameter β_2

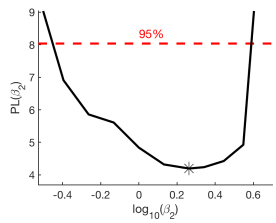

Parameter β_3

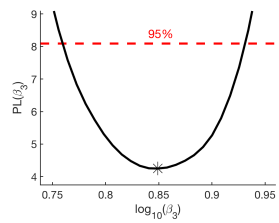

Parameter β_4

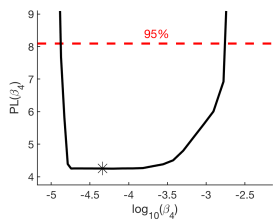

Parameter β_5

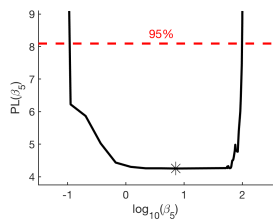

Parameter β_6

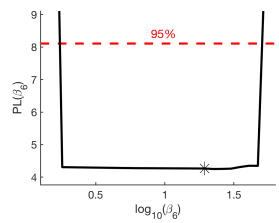

Parameter β_7

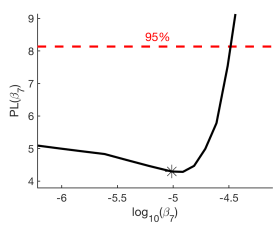

Parameter β_8

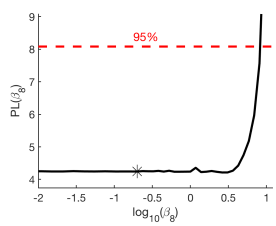

Parameter β_9

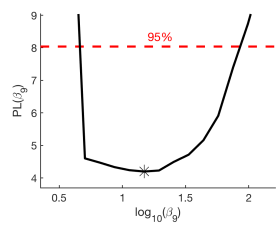

Parameter β_{10}

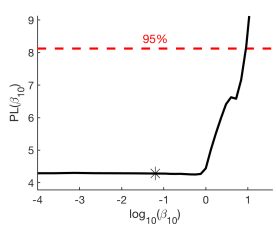

Parameter β_{11}

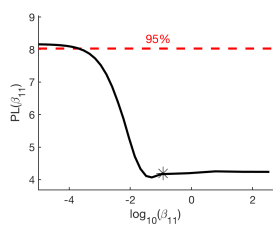

Parameter β_{12}

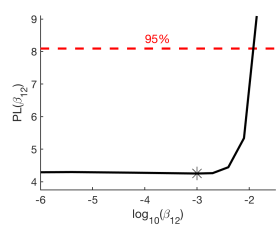

Parameter β_{13}

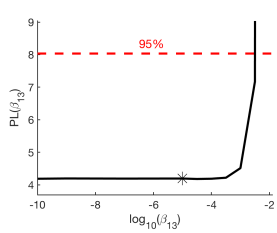

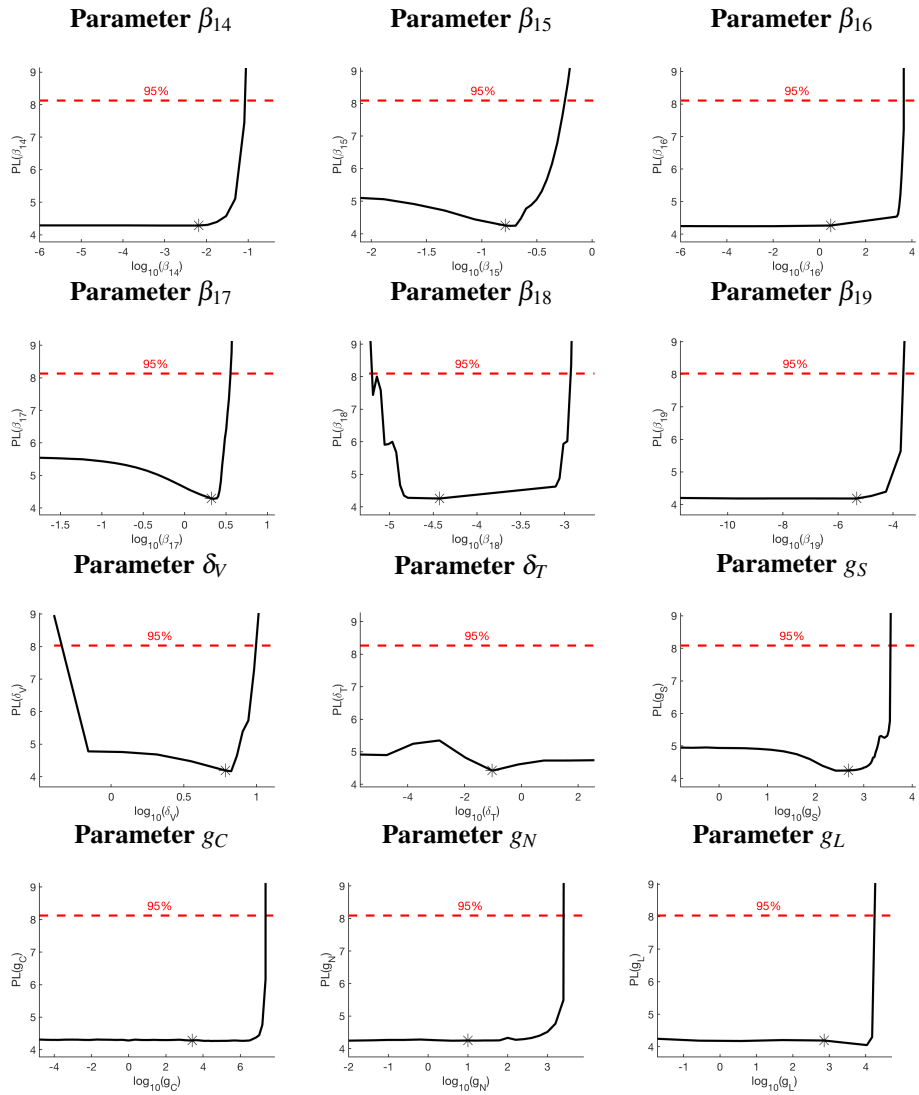

Figure C.1: Profile likelihoods from the identifiability analysis.

Appendix D

Likelihood Profiles from extended identifiability analysis

Here the profile likelihoods for the extended identifiability analysis is presented. The analysis was performed on parameter β_1 to g_L. In the figures the asterisks mark the parameter value that yielded the best fit and the red dashed line demonstrates the 95% confidence level.

Parameter β_1

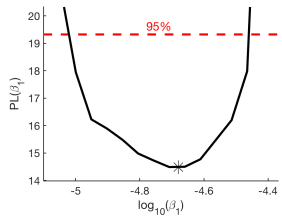

Parameter β_2

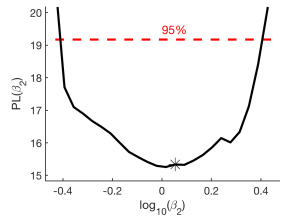

Parameter β_3

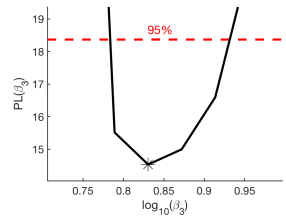

Parameter β_4

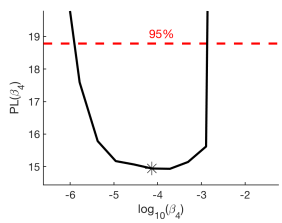

Parameter β_5

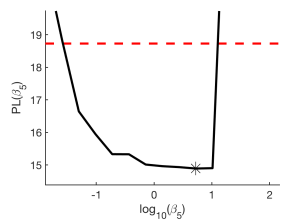

Parameter β_6

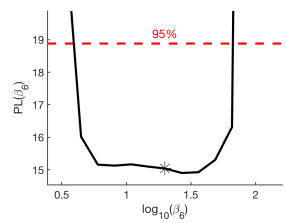

Parameter β_7

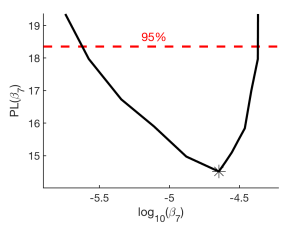

Parameter β_8

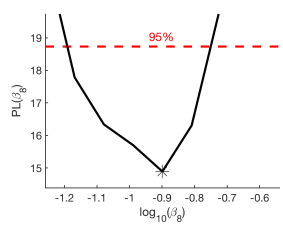

Parameter β_9

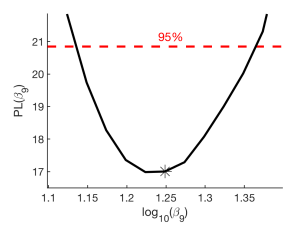

Parameter β_{10}

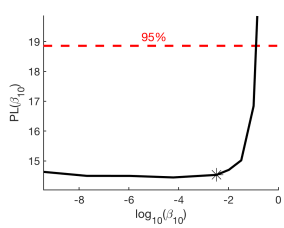

Parameter β_{11}

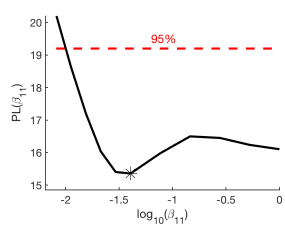

Parameter β_{12}

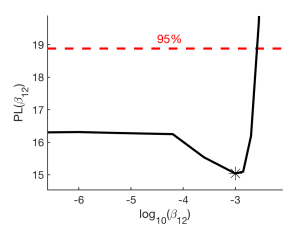

Parameter β_{13}

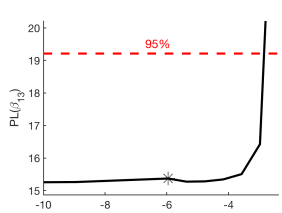

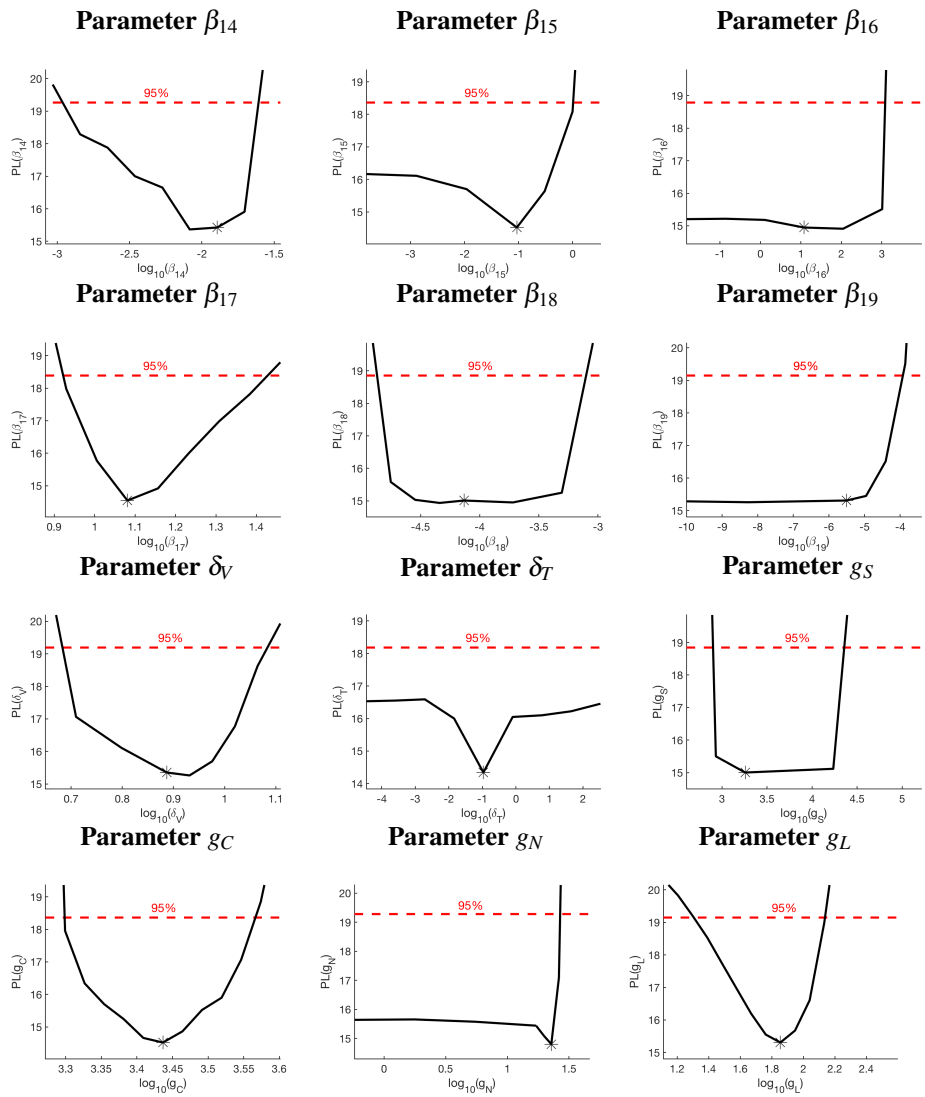

Figure D.1: Profile likelihoods from the extended identifiability analysis.